In-Situ Characterization of Spinel Nanoceramic Suspensions

Tamar Kadosh

In-Situ Characterization of Spinel Nanoceramic Suspensions

Research Thesis

in partial fulfillment of the requirements for the
degree of Master of Science in Materials Engineering

Tamar Kadosh

Submitted to the Senate of the Technion - Israel Institute of Technology

Tammuz 5770 Haifa July 2012

The research thesis was done under the supervision of Wayne D. Kaplan, Yeshayahu Talmon and Yachin Cohen in the Department of Materials Engineering.

I wish to thank Prof. Wayne Kaplan, Prof. Yeshayahu (Ishi) Talmon and Prof. Yachin Cohen for their dedicated and professional guidance. I would also like to thank Mrs. Judith Schmidt and Mrs. Berta Shdemati for their support. I thank Mr. Liron Issman and Mrs. Na'ama Elisar for their assistance and for teaching me the SEM method.

I would like to kindly acknowledge my supervisors, colleges and friends in Rafael Mr. David Gorni, Mr. Shimshon Bar-ziv and Mrs. Anat Shenhar for fruitful discussions and valuable suggestions.

I am grateful to Mr. Leonid Zisman for performing SLS measurements and Dr. Gennady Shter for performing MIP measurements.

I would like to acknowledge Prof. Simon Brandon and Prof. Michael Shapira are acknowledged for discussions on particle movement under laminar shear flow.

The generous financial support of Rafael Ltd and the Technion is gratefully acknowledged.

I thank my family for their endless faith and support.

Table of contents

1 Introduction 4

1.1 Spinel – Structure, Properties and Applications 4

1.1.1 Crystal Structure 4

1.1.2 Properties 5

1.1.3 Applications 6

1.2 Ceramic Processing 7

1.3 Aqueous Suspensions 9

1.4 Suspension Characterization Methods 12

1.4.1 Particle Sizing Using Static Light Scattering (SLS) 12

1.4.2 Zeta Potential Measurements 12

1.4.3 Rheological Measurements 13

1.4.4 Wet Specimen Imaging and Cryo-SEM 15

1.4.4.1 Conventional SEM 15

1.4.4.2 Environmental SEM (ESEM) 15

1.4.4.3 WetSEM^{TM} Capsules 16

1.4.4.4 Cryo-SEM 16

1.5 Green Compact Characterization Methods 18

1.5.1 Density Measurement (using Archimedes' Principle) 18

1.5.2 Mercury Intrusion Porosimetry 19

2 Research Objectives 20

3 Experimental Methods 21

3.1 Preparation of Suspensions 21

3.2 Suspension Characterization Methods 21

3.2.1 Particle Size Distribution 21

3.2.2 Zeta Potential Measurements 21

3.2.3 Rheological Measurements 22

3.2.4 Cryo-SEM 22

3.3 Green Compact Characterization 26

3.3.1 Green Density from Archimedes' Principle 27

3.3.2 Mercury Intrusion Porosimetry 28

4 Results 29

4.1 Powder Characterization 29

Table of contents

4.2 Zeta Potential 30
4.3 Rheological Measurements 31
4.4 Cryo-SEM 33
4.5 Green Compact Density and Porosity 37
5 Discussion 39
6 Summary and Conclusions 44
7 Suggested Future Research Directions 46
References 47

List of figures

Figure 1.1: Schematic drawing of the spinel crystal structure. 4
Figure 1.2: Transmittance vs. wavenumber and wavelength of spinel, AlON, sapphire and yttria. 5
Figure 1.3: Temperature dependence of the emittance of spinel, AlON, sapphire and yttria.[4] 5
Figure 1.4: Perforation tests on composite targets with different front tails.[5] 7
Figure 1.5: A flow chart showing the production process of ceramic materials by slip casting. 8
Figure 1.6: Schematic illustration of the suspension morphology (right) resulting from the correlative total inter-particle potential energy (left).[12] 11
Figure 1.7: Viscosity vs. shear rate: (a) Newtonian system; (b) Pseudo-plastic behavior; and (c) Dilatant behavior. 14
Figure 1.8: Viscosity vs. time, under constant shear rate. 14
Figure 1.9: Mercury in contact with a porous material.[40] 19
Figure 3.1: The controlled environmental chamber used for preparing specimens. 23
Figure 3.2: Photograph of the "Sandwich" assembly, where a 5μl droplet of suspension is placed between two gold planchettes. 23
Figure 3.3: Photograph of the liquid ethane bath and sample used for vitrification. 24
Figure 3.4: Photograph of the "Sandwich" being inserted into the sample holder, under liquid nitrogen (not seen in the picture) 25
Figure 3.5: Photograph of the sample holder which upon opening fractures the vitrified sample. 25
Figure 3.6: Photograph of the spinel suspension cast on: a) a dry mold; and b) a wet mold. 27
Figure 3.7: Photograph of the spinel green compacts on porous alumina molds. 27
Figure 4.1: Particle size distribution of the spinel powders, after different times of ball-milling, acquired from static laser scattering (SLS). 29
Figure 4.2: Zeta potential of spinel powder in water (~150ppm) at different pH levels. The spinel IEP is at pH~11.8. 30
Figure 4.3: Zeta potential of the investigated spinel suspension at different pH levels. 31
Figure 4.4: The viscosity vs. shear rate for a 60 wt.% spinel suspension. 32

List of figures

Figure 4.5: Viscosity versus time for a 60 wt.% spinel suspension, measured using Brookfield spindle number 3 at 60 rpm. 33
Figure 4.6: Secondary electron cryo-HRSEM micrograph, based on a combined signal from in-lens and conventional secondary electron detectors, of a 60 wt.% spinel suspension without aging. 34
Figure 4.7: Secondary electron cryo-HRSEM micrograph, based on a combined signal from in-lens and conventional secondary electron detectors, of a 60 wt.% spinel suspension after 0.5 hour aging. 34
Figure 4.8: Secondary electron cryo-HRSEM micrograph, based on a combined signal from in-lens and conventional secondary electron detectors, of a 0.6 wt.% suspension diluted from the original 60 wt.% suspension. 35
Figure 4.9: The micrograph in Figure 4.8 after processing using the ImageJ software. The thin lines, indicated by arrows, are the boundaries between elementary particles in the suspension. 36
Figure 4.10: Results from image analysis after processing. Most of the elementary particles are between 25 to 55 nm in diameter. 36
Figure 4.11: Incremental volume of pores versus pore diameter. 37
Figure 4.12: Normalized cumulative volume of pores versus pore diameter. 38

List of tables

Table 1: Optical and mechanical parameters and properties of spinel.[4] 6
Table 2: Comparison between physical characteristics of two different cryogens. ... 18
Table 3: Impurities in the initial spinel powder, as determined from ICP. 21
Table 4: Green compact average density, calculated by Archimedes method and by porosimetry results, for 10-12 specimens casted from as-milled and aged suspensions..... 38

ABSTRACT

In this study an approach to characterize ceramic colloidal suspensions has been developed, based on vitrification of aqueous ceramic suspensions and micro-structural characterization by cryogenic-temperature scanning electron microscopy (cryo-SEM), augmented by conventional rheological measurements. The flocculation phenomenon in as-milled and aged Mg-spinel ($MgAl_2O_4$) aqueous suspensions was characterized. A microstructure based on hard particle agglomerates separated by long-chain deflocculant molecules was directly observed, and correlated to the rheological properties of the suspension. Several levels of flocculation were detected as function of suspension preparation conditions. While suspensions at solid-loading levels appropriate for ceramic processing cannot be characterized by conventional particle size measurement techniques, cryo-SEM can be used to measure characteristic sizes, and distinguish between agglomerated and flocculated particles, opening a new approach for optimizing solid-loading conditions for slip-casting, in terms of viscosity and green density. “Green compacts” were cast from the investigated suspensions, and their density and pore size-distribution were characterized using Archimedes' principle and mercury intrusion porosimetry, respectively. Comparing green compacts cast from fresh and aged suspension, similar densities and pore size distributions were found. Hence, it was concluded that the duration of the drying process (and the fixation of the suspended particles in the cast), is longer than the aging time of the cast suspension.

List of symbols and abbreviations

A	dry weight of green compact (used for density calculation)
a	lattice parameter
AlON	Aluminum oxynitride
B	wet weight of green compact (used for density calculation)
BET	Brunauer, Emmet, Teller
C	weight of green compact, when immersed in water (used for density calculation)
D_A	total areal density
D_p	pore diameter
d	particle diameter
E	Young's Modulus (GPa)
E_{pT}	total inter-particle potential energy
E_{vdW}	potential energy due to van der Waals interactions between particles
E_{elect}	energy due to electrostatic interactions between the particles
E_{steric}	steric potential energy stems from the interactions between adsorbed organic additives
$E_{structural}$	structural potential energy between particles
E_T	thermal energy resulting from thermal fluctuations
EDS	energy dispersive spectroscopy
ESEM	environmental SEM
FCC	face centered cube
HV10	hardness Vickers under 10kg load (GPa)
HRSEM	high resolution scanning electron microscopy
IEP	iso-electric point
k	thermal conductivity (W/m·K)
k_B	Boltzmann constant
P	applied pressure used for mercury intrusion
%P	percentage of open porosity
ppm	parts per million
$RI_{0.5}$	refractive index @ λ=0.5μm
RI_4	refractive index @ λ=4μm
S	mean strength (MPa)

S_{BET}	specific surface area
STP	standard temperature and pressure
T	temperature
%TD	percentage of theoretical density
t_4	transmittance @ λ=4μm
V_I	volume backfilled with mercury under low pressure (not attributed by pores)
V_{green}	Volume of green compact
$V_{porosity}$	Volume of pores in the green compact
V_T	total cumulative pore volume
vdW	van der Waals
α	thermal expansion coefficient (10^{-6} K^{-1})
γ	mercury surface tension
$\dot{\gamma}$	shear rate
ζ	zeta potential
η	viscosity
θ	contact angle between mercury and pore opening
λ	wave length
ν	Poisson's Ratio
ρ	$MgAl_2O_4$ theoretical density (ρ=3.58gr/cm^3)
τ	shear stress

1 Introduction

1.1 Spinel – Structure, Properties and Applications

Transparent polycrystalline ceramics have received much attention in recent years, due to their applications in systems requiring a combination of optical properties with high mechanical strength and impact resistance. Magnesium aluminate spinel ($MgAl_2O_4$) is one of the most favorable candidates, both for armor and optical applications.

1.1.1 Crystal Structure

Spinel is a cubic crystal with 56 atoms per unit cell, which belongs to the space group $Fd\bar{3}m$. Magnesium aluminate spinel (from this point referred to as spinel) has a lattice parameter of a=8.085Å. It is composed of alumina (Al_2O_3) and magnesia (MgO) in a ratio of 1:1 (molar). The structure can be described as follows: all oxygen ions are located in the FCC sites (the cube is marked in red lines), whereas the cations are located in the FCC interstitial sites: all the trivalent cations (Al^{+3}) occupy half of the octahedral sites, while all the divalent cations (Mg^{+2}) occupy 1/8 of the tetrahedral sites (see Figure 1.1).[1,2]

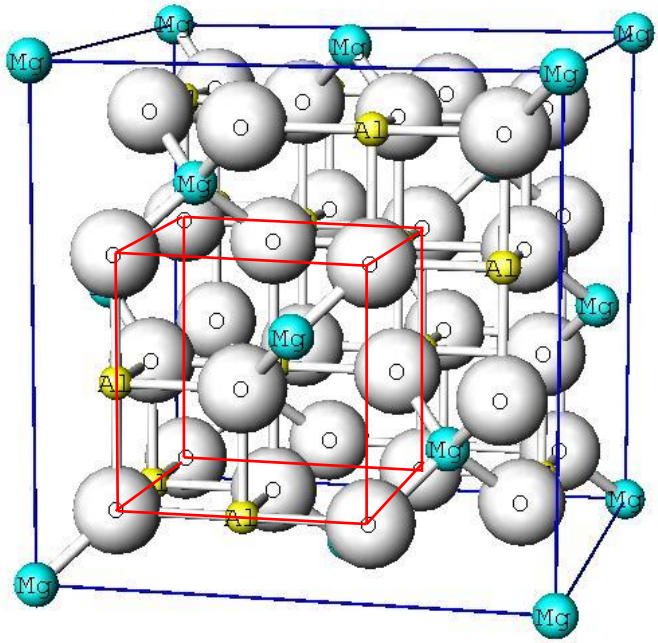

Figure 1.1: Schematic drawing of the spinel crystal structure.

1.1.2 Properties

Spinel is superior to AlON (aluminum oxinitride) and sapphire (single crystal α-Al_2O_3) in terms of transmission in the infra-red range (3-5μm),[3] and maintains its superiority at high temperatures (see Figure 1.2 and Figure 1.3).

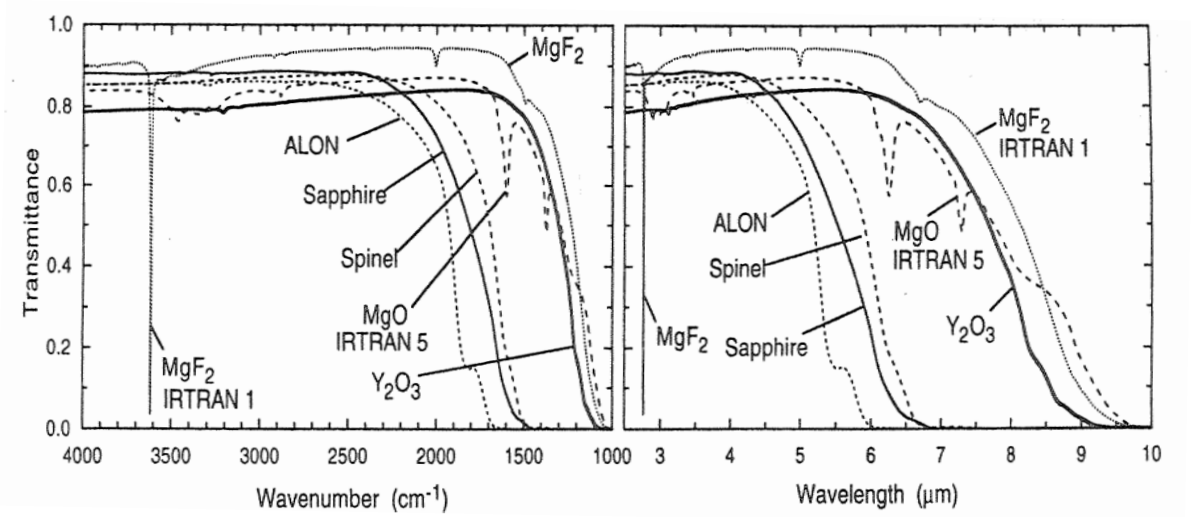

Figure 1.2: Transmittance vs. wavenumber and wavelength of spinel, AlON, sapphire and yttria.[4]

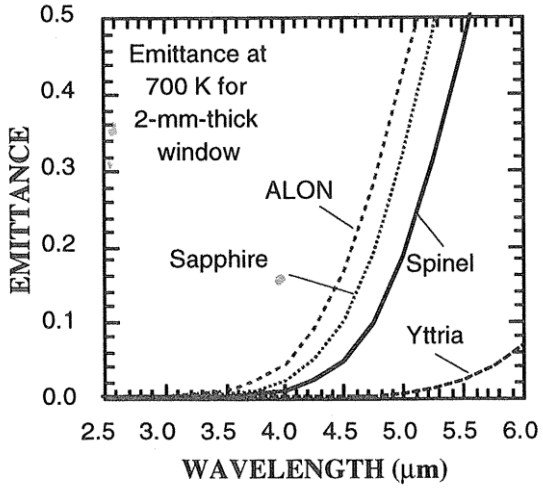

Figure 1.3: Temperature dependence of the emittance of spinel, AlON, sapphire and yttria.[4]

Spinel also has better ballistic efficiency, and a lower predicted cost of production compared to sapphire.[5] The optical and mechanical parameters and properties of spinel are presented in Table 1.

	Property / Parameter	Value
Optical Properties	$RI_{0.5}$ - Refractive Index @ λ=0.5μm	1.723
	RI_4 - Refractive Index @ λ=4μm	1.639
	t_4 – Transmittance @ λ=4μm	0.889
Mechanical Properties	S - Mean Strength (MPa)	190-250
	HV10 - Hardness (GPa)	14.5–15.0
	α – Thermal expansion coefficient (10^{-6} K^{-1})	5.6
	ν - Poisson's Ratio	0.26
	E – Young's Modulus (GPa)	193
	k – Thermal conductivity (W/m·K)	14.6

Table 1: Optical and mechanical parameters and properties of spinel.[4]

1.1.3 Applications

Due to its good transmittance in the visible and IR range, spinel can be used for windows for detectors. Spinel can also be applicable as transparent armor, since it has high hardness, leading to high ballistic strength. Ballistic strength is defined as the shielding effect of a ceramic tile in front of some backing. Figure 1.4 presents results of perforation tests performed on composite targets of transparent ceramic or glass front tiles, with backings of a constant thickness (60mm of soda-lime floatglass and polycarbonate). The total areal density (D_A) of the composite target is the weight per unit area, required to stop the projectile. A lower value of D_A indicates better ballistic efficiency. In other words, a lighter window can stop the same threat (projectile). D_A of a target can be calculated by summing the tile's density multiplied by its thickness, and the backing density multiplied by its thickness (constant for all tests). Although the density of most glasses is lower than the density of crystalline ceramics, the total areal densities of the ceramic targets are lower, which means that ceramics are more efficient as armor. A 2mm spinel front reduces the D_A by 50% to 70%.[5]

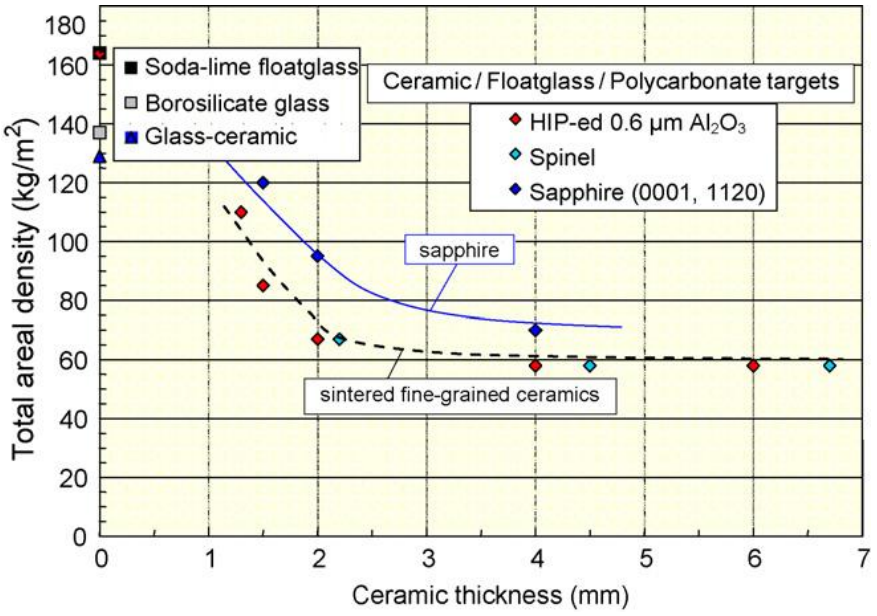

Figure 1.4: Perforation tests on composite targets with different front tails.[5] The total areal density of composite targets is reduced by thin ceramic fronts.

1.2 Ceramic Processing

Non-sintered (green) compacts of spinel are commonly produced by the dry-press method[6,7] but can also be produced by "wet" methods, such as slip-casting[8,9] or gel-casting[10]. The latter methods provide a variety of possible geometries, such as curved windows and domes, which are difficult to form using dry-press methods. An additional advantage of wet methods is the potential to obtain more homogeneously packed green compacts, due to the greater ease with which the particles can slide over one another and rearrange in the wet state.[11] A homogeneous microstructure in the green state is extremely important when transparency in the fully sintered state is required, since heterogeneities (defects) introduced in any stage of the fabrication process can detrimentally affect densification.[12,13] The degree of optical transmission through polycrystalline ceramics strongly depends on absorption and scattering by pores,[5] making removal of residual porosity a critical step of the sintering process.

A schematic flow chart of ceramic processing using slip casting is presented in Figure 1.5. The slip (or suspension) is formed by dispersing the powder in a fluidic media and adding the required dispersants. After the de-agglomeration process, the suspension is cast into a mold to create a green compact. Plaster can be used as the

porous platform, delineated with sealed side-walls. The green body is then dried, mostly via capillary forces exerted by the pores of the mold. The green body is heated to dispose of all organic ingredients and then sintered to obtain only closed pores. The pre-sintered body is then isostatically pressed using inert gas at high temperature to sinter to full density.

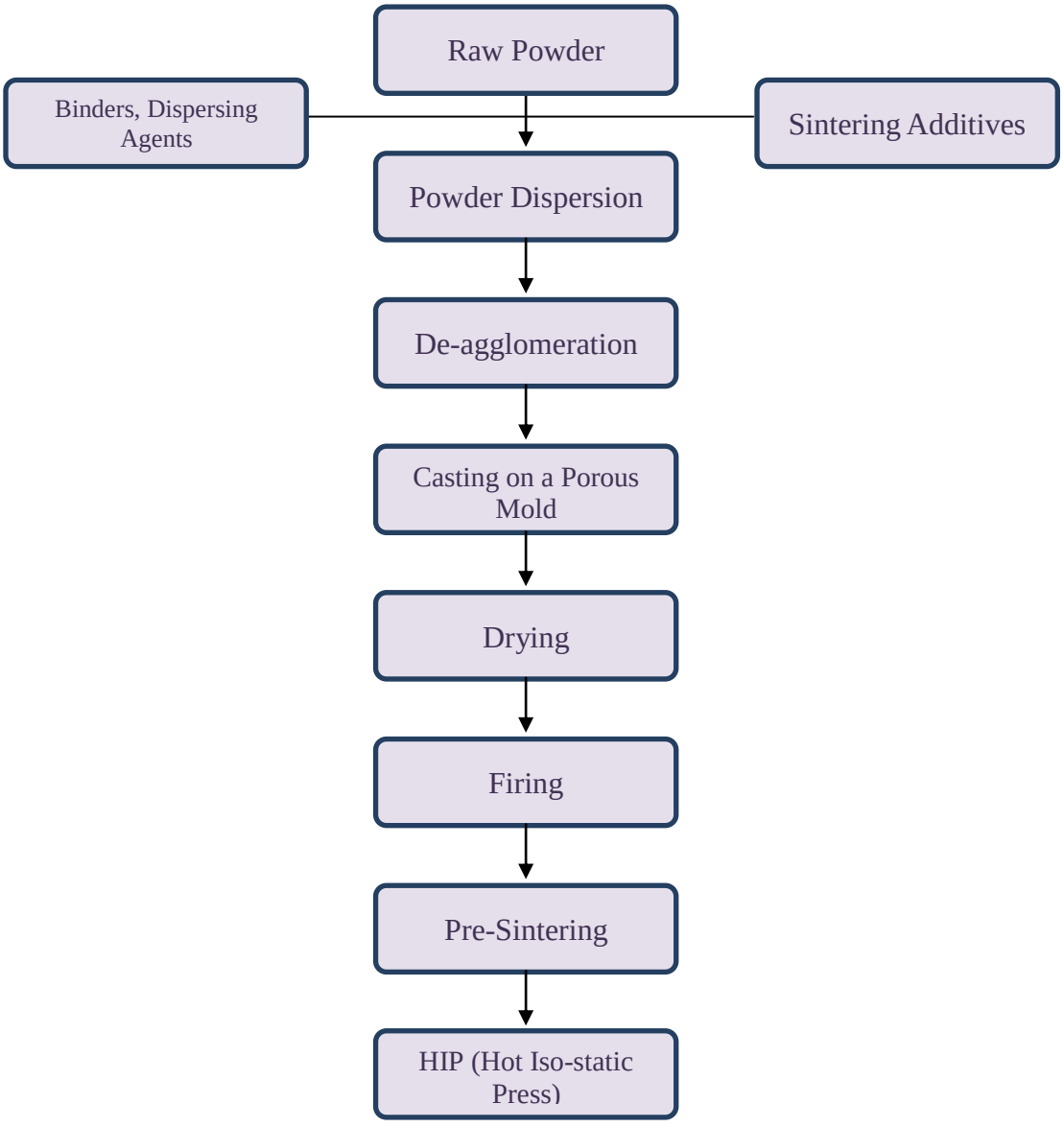

Figure 1.5: A flow chart showing the production process of ceramic materials by slip casting.

1.3 Aqueous Suspensions

The key for successful wet-forming, and the minimization of heterogeneities in the green state, is the ability to produce a well-dispersed, high solid content, low viscosity suspension.[14] These requirements are problematic when sub-micron (nano) ceramic powders are used, due to their high specific surface area, which promotes flocculation. A floc is an agglomerate with a porous microstructure, which forms in a liquid suspension.[15] The particles of a floc are held together by long-range van der Waals forces,[16] or by organic flocculation agents[12]. It is generally true that particles with a large surface area tend to cause agglomeration and flocculation may lead to porous, poorly packed green structures and reduced green densities.[17]

Colloidal suspensions can be prepared in the dispersed, weakly flocculated or strongly flocculated states, as shown schematically in Figure 1.6.[12] Dispersed particles interact: they attract and/or repel each other. The interaction intensities depend on the distance between the particles. Flocculation depends on the total inter-particle forces or the total potential energy of the dispersed particles. The thermal energy resulting from thermal fluctuations of the particles is referred to as $E_T=k_BT$. A total potential energy higher than that value would enable repulsion between the particles, whereas a lower potential energy means a reduction of the mean distance between particles and thus aggregation. In other words, a dispersed state is reached when the total inter-particle forces are repulsive and the energetic barrier for particle approach is much higher than k_BT. In the weakly flocculated state, the particles are held together as a weak net structure and an equilibrium separation distance exists between them. A well of potential energy exists at short particle-particle distances leading to aggregation. In the strongly flocculated or coagulated state, particles aggregate due to a deep primary minimum of potential energy. The particles form a touching network or clusters in suspension.

The total inter-particle potential energy (E_{pT}) can be expressed as:

$$E_{pT} = E_{vdW} + E_{elect} + E_{steric} + E_{structural} \qquad \textbf{(1)}$$

E_{vdW} is the potential energy due to van der Waals (vdW) long-range interactions, which often (depending on the Hamaker coefficient) can result in attractive forces. The vdW forces result from permanent or induced dipoles on the

molecules.[16] E_{elect} is the energy due to electrostatic interactions between the particles, caused by the charge on the surface of the particles, and is usually repulsive because the surfaces have the same electric charge. E_{steric} is the energy resulting from interactions between relatively large adsorbed organic molecules. A dispersant added to the suspension will be adsorbed to the particles' surface. The adsorbed polymers prevent particles from approaching each other. When the polymer concentration is not optimized (either too high or too low), it can cause the opposite interaction, i.e. the polymers adsorbed to different particles attract and stick together forming a network of particles. This phenomenon is called "bridging".[18] A repulsive potential energy can be also induced by adding a polar polymer, e.g. polyacrylate. The polymer is favorably adsorbed to the surface of the particle when they carry opposite charges. The polymer then acts to repel particles from each other via both electric and steric forces (electro-steric repulsion forces). $E_{structural}$ is the energy resulting from the presence of non-adsorbed species in solution that may encourage either attraction or repulsion interactions.[12]

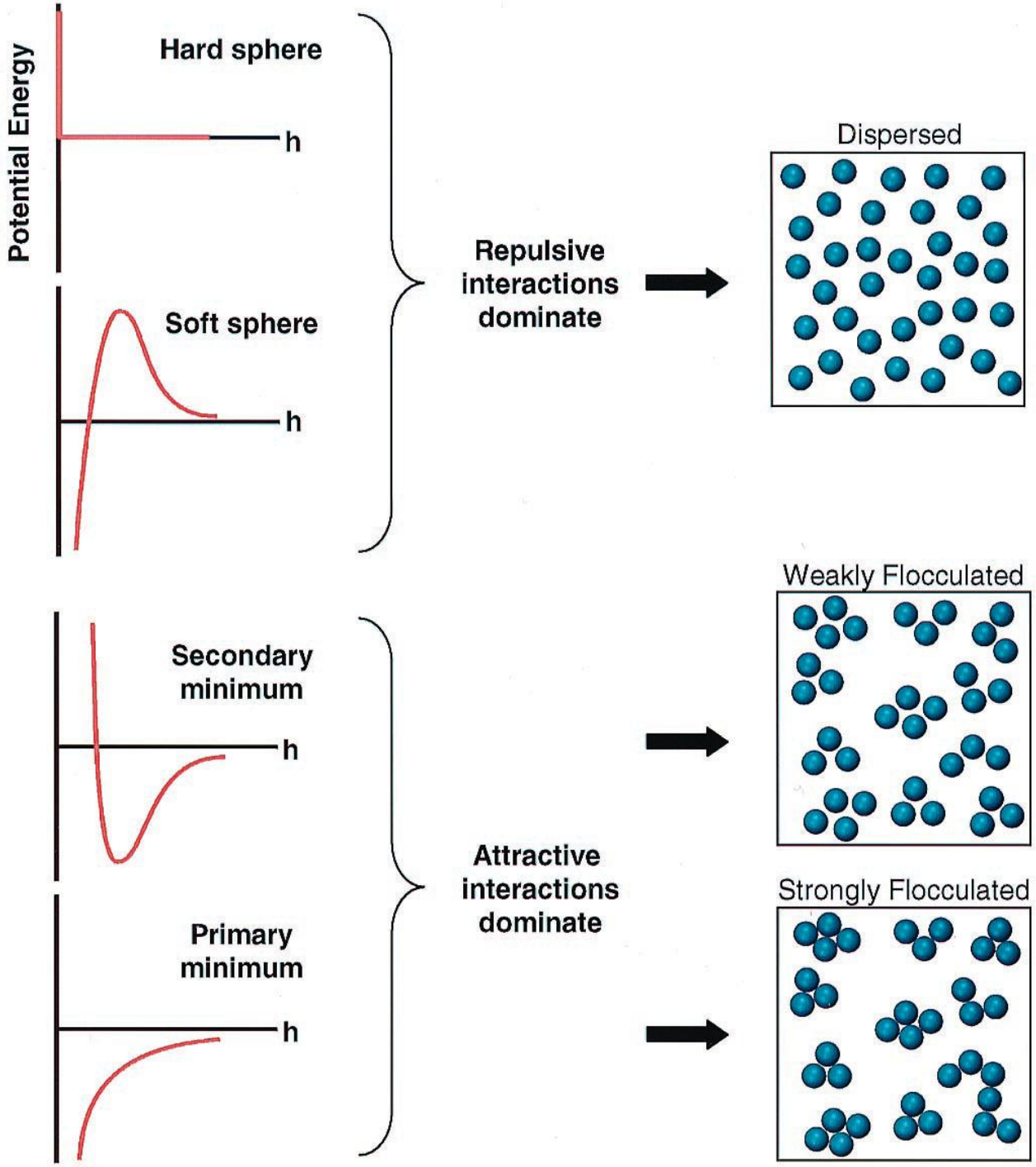

Figure 1.6: Schematic illustration of the suspension morphology (right) resulting from the correlative total inter-particle potential energy (left).[12]

1.4 Suspension Characterization Methods

As explained previously, the suspension quality affects the microstructure of the green compact. An appropriate green microstructure contributes to the sintering process and leads to a dense product without porosity. The microstructure of the suspension can indicate about its quality, therefore it is extremely important to characterize it. Most of the following methods are well established as suspension characterization techniques, except for cryo-SEM, which is suggested here as a complimentary method, especially suitable for high solid load suspensions.

1.4.1 Particle Sizing Using Static Light Scattering (SLS)

Laser diffraction is a method used to characterize the particle size distribution in a suspension, by measuring the scattered intensity as a function of the scattering angle. It covers a size range of nanometers to millimeters and the results are reproducible. For simplicity, the particles are assumed to be spherical and the representative size is their diameter. A light source generates a monochromatic beam. The beam passes through several optical components to form a Gaussian intensity distribution, and illuminates the suspended particles. Particles scatter light with angles and intensities correlated to their size. An array of detectors collects the scattered light.[19] Complex mathematical algorithms, based on the Mie theory of light (or more accurately the Mie solution to Maxwell's equations), are used to calculate the particle size distribution responsible for the detected light scattering. The method obviously requires a transparent medium.

1.4.2 Zeta Potential Measurements

The sign and magnitude of the surface charge of colloidal particles in contact with an aqueous solution affect the stability of colloidal dispersions, their rheological properties, and their ability to adsorb ions from solution. Therefore, the point of zero charge (PZC) or the iso-electric point (IEP) is an important property of colloids.[20]

In solution, the surface charge (which can be inherent to the particles or the result of ion adsorption) is shielded by a diffuse layer of solvated counter-ions. The electrostatic surface potential is termed the zeta potential (ζ) and is highly dependent

on the immediate environment. Together, the fixed surface charge and diffuse layers are termed the “double layer”. [21]

Zeta potential measurements can be used to estimate the stability of suspensions in terms of electrical repulsion.[22] When dispersing oxide powders in water, there is a surface reaction leading to the formation of M-OH type hydroxide groups that can dissociate as acids or bases:

$$M\text{-}OH_{surface} \leftrightarrow M\text{-}O^{-}_{surface} + H^{+} \quad \text{in basic slurry} \qquad \textbf{(2)}$$

$$M\text{-}OH_{surface} + H^{+} \leftrightarrow M\text{-}OH_2^{+}{}_{surface} \quad \text{in acidic slurry} \qquad \textbf{(3)}$$

The number of negative, neutral, or positive surface sites is of function of pH. At low values of pH, positive surface sites dominate, and vice versa. The net charge density of the particle is determined by the sum of the overall surface charge, and can be determined from zeta potential measurements for *dilute* (transparent) suspensions.[23]

1.4.3 Rheological Measurements

A suspension’s microstructure and stability can be inferred from the observed rheological behavior. Therefore, rheological measurements are an important tool when trying to estimate the suspension quality. It is known that flocculation causes an apparent rheological behavior of increasing viscosity with time, often termed "aging".[24] For this reason, viscosity measurements can also indicate the level of flocculation.[25]

Fluid based systems can be generally divided into two groups: Newtonian and non-Newtonian. The viscosity of Newtonian systems is constant with shear rate, shear stress and time under shear (see (a) in Figure 1.8 and the constant function in Figure 1.7), whereas the viscosity measured for non-Newtonian systems is subjected to these factors. The relation between viscosity (η), shear rate ($\dot{\gamma}$) and shear stress (τ) for all flow behaviors is given by:

$$\tau = \eta\dot{\gamma} \qquad \textbf{(4)}$$

The type of flow behavior observed under steady shear can differ, depending on the suspension composition and stability. Pseudo-plastic or shear-thinning behavior occurs when the viscosity decreases with shear rate (see curve (b) in Figure

1.7). Dilatant or shear-thickening behavior occurs when the viscosity increases with shear rate (see curve (c) in Figure 1.7).

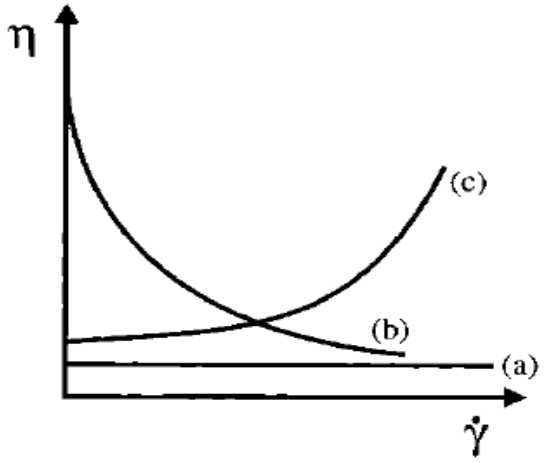

Figure 1.7: Viscosity vs. shear rate: (a) Newtonian system; (b) Pseudo-plastic behavior; and (c) Dilatant behavior.

Flow behavior can also be time dependent. Thixotropic systems exhibit an apparent viscosity that decreases with time under shear (see Figure 1.8) and the opposite behavior is referred to as rheopexy.[12]

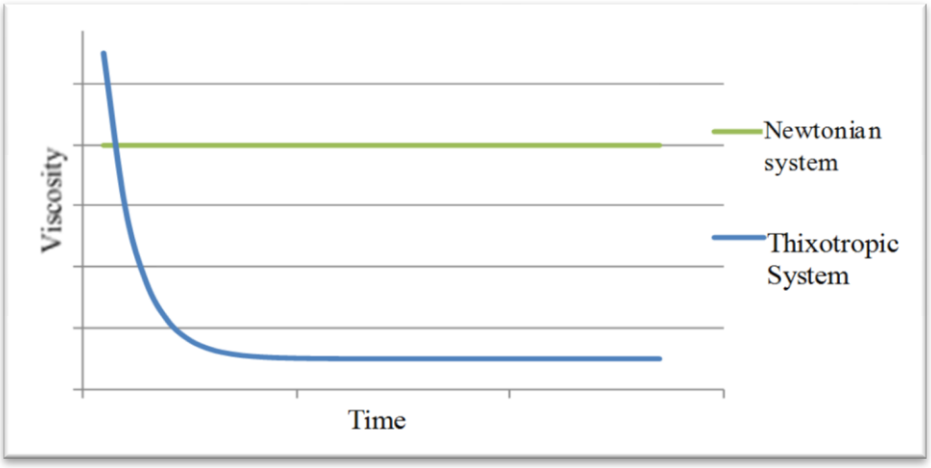

Figure 1.8: Viscosity vs. time, under constant shear rate.

Despite flocculation phenomenon being well established for ceramic suspensions in the literature, to the best of the authors' knowledge it has rarely been directly observed using microscopy.[26,27]

1.4.4 Wet Specimen Imaging and Cryo-SEM

Materials that are liquids at STP (standard temperature and pressure), will not be stable under high vacuum conditions, used in the chamber of an electron microscope. When trying to characterize suspended particles in a liquid phase using SEM, there are several possible modes of operation, and these are discussed in the following.

1.4.4.1 Conventional SEM

For conventional SEM, sample drying is obligatory. When trying to preserve the morphology of biological tissues, fixation can be applied. Fixation is a technique that quickly arrests biological activity and stabilizes cellular components with minimal distortion of conformational and spatial relationships between cellular constituents. As inferred, the fixation procedure and the dehydration process increase the possibility of introducing artifacts.[28]

1.4.4.2 Environmental SEM (ESEM)

Environmental SEM (ESEM) works in a gaseous atmosphere and allows imaging wet samples. The electron gun is maintained at high vacuum, while the chamber where the samples are held, is in lower vacuum conditions. The separation is possible thanks to a special design of the electron optical column that allows for differential pumping, where the column is divided into different pressure zones separated by pressure limiting apertures. The low vacuum atmosphere in the chamber minimizes liquid evaporation from the sample, compared to a high vacuum atmosphere, thus preserving the wet state.[29] The energetic electron beam penetrates the gas (commonly water vapor), while scanning the specimen. Electrons scattered from the specimen (backscattered electrons) encounter gas molecules, causing them to release secondary electrons. Since each backscattered electron can generate thousands of secondary electrons, the gas amplifies the original electron signal from the specimen. At the same time, the positive ions resulting from this cascade process drift towards the specimen surface and thereby help to compensate for negative charge build-up. Hence, non-conductive samples can be imaged without the need for a conductive coating. Minimal sample preparation is required, as fixation, hydration and coating procedures are not needed. This reduces the amount of artifacts

introduced by specimen preparation. However, the radiation damage is enhanced by the poor vacuum and deteriorates the resolution.[28]

1.4.4.3 WetSEM™ Capsules

Wet scanning electron microscopy (WetSEM™) capsules comprise an electron transparent membrane enabling the imaging and elemental analysis of liquid samples. The stainless steel capsules were designed by Quantomix™ (Israel), in a way that wet samples placed in them will not evaporate while still releasing electrons and photons (X-ray signals used for EDS analysis). The wet sample in the capsule can be imaged in a standard SEM. High accelerating voltages of 20–30 kV should be applied, to allow for sufficient penetration depths, the generation of backscattered electrons, and to reduce beam interactions within the capsule membrane. To reduce damage to the membrane of the capsules, electron beam currents and excessive dwell times of the beam on small areas during imaging, should be minimized. Therefore, imaging at high magnification is limited.[30] Given these limitations, the capsule enables observation of aggregation and settling processes of unstable suspensions, gel formation processes, and other progressing phenomena. The main disadvantage of the technique is an artifact referred to as the "wall effect", where due to the vacuum tight membrane of the capsule, smaller particles tend to accumulate near the membrane.[31]

1.4.4.4 Cryo-SEM

Cryo-SEM is the only SEM option that preserves the microstructure of liquid samples without limiting resolution, as long the sample is prepared following a specific and meticulous method. Cryogenic scanning electron microscopy (cryo-SEM) is a powerful tool for characterizing the morphology of samples containing both liquids and solids. It enables direct observation of the microstructure of hydrated samples. The method was originally used in biological research to observe bacteria, animal and plant cells.[32] It was also used in the field of geology, to mimic and investigate the mechanism of a phenomenon called columnar jointing. Menger et al. characterized the gel structure formed by a gemini surfactant of an amphiphilic nature.[33] The molecule self-assembles in water at varied concentrations, into a submicroscopic network of polygonal columns, which are filled first with water, and

later with vitreous ice. The columns create a skeleton, providing a template for the unusual fracturing of the vitreous ice, into a columnar morphology. This fracturing resembles the formation of columnar jointing in geological structures.

In materials science, cryo-SEM was used to observe suspensions of polymers (latex)[34], silica[35,36] and clays[26,37]:

Omer et al. used cryo-SEM to investigate the structural evolution during silica-based mesoporous material formation, starting from the hexagonal phase to the final cubic phase. They revealed the existence of an intermediate stage when the hexagonal phase evolves to a perforated layer, which later develops into a bicontinuous structure. The final cubic phase was found to be formed within the layers.[35]

Wyss et al. analyzed the microstructure of spherical silica particles of half micron diameter, as an aqueous suspension. They induced coagulation using urea hydrolysis, and compared the gel structure to the initial (stable) suspension. It was found that the stable suspension forms a homogeneous microstructure, whereas the de-stabilized one is inhomogeneous.[36]

Cryogenic electron microscopy of water-based samples (suspensions) requires vitrification, where the liquid media of the suspension (commonly water) is rapidly cooled to avoid distortion of the sample morphology by ice crystal formation. The cooling rate depends on the temperature of the cryogen, the rate of immersing the sample in the cryogen (the plunging speed), the specimen and cryogen heat conduction properties, and the sample's volume.

The cryogen used for specimen vitrification has to be selected carefully. As presented in Table 2, liquid ethane has a much higher heat capacity than nitrogen. Furthermore, its viscosity is lower and it has a larger difference between its melting point and boiling point compared to nitrogen, which inhibits boiling. The heat transfer coefficient is much higher in liquid ethane at its freezing point than in a film of evaporated nitrogen, leading to a higher cooling rate, thus minimizing freezing artifacts.[38] Therefore, ethane is regarded as superior to nitrogen and other liquid cryogens. However, ethane should not be used for specimens based on organic liquids which may dissolve in it, thus destroying the microstructure of the sample.[39]

Properties @ ambient pressure / Cryogen	Nitrogen	Ethane
Melting point	-210°C	-182.8°C
Boiling point	-195.7°C	-88.6°C
Heat Capacity @ T= -150°C	~29 J/(mol K)	68.5 J/(mol K)
Heat Capacity @ T= -196°C	57.1 J/(mol K)	

Table 2: Comparison between physical characteristics of two different cryogens.

Vitrified samples should be fractured to expose a cross-section. Then, some of the vitrified solvent should be sublimated to increase topographic contrast. To reduce charging, a thin conducting film should be deposited on the fracture surface. A cold-stage in a high-resolution scanning electron microscope is then required for characterization.

1.5 Green Compact Characterization Methods

Suspensions used for casting on porous media form green, porous compacts, as described in section 1.2. Their characterization, prior to sintering, is important to understand the consolidation process and its influence on the microstructure of the final sintered body.

1.5.1 Density Measurement (using Archimedes' Principle)

A compact of a material of known theoretical density is weighed when dry (A), wet (B), and immersed in water (C), to determine its density. This process only works for a green compact which will not disperse in water, and is usually applied to (bisque) fired or sintered samples. This method is based on Archimedes' principle, where any object, wholly or partially immersed in a fluid, is buoyed by a force equal to the weight of the fluid displaced by the object. For a sunken object, the volume of displaced fluid is the volume of the object. Therefore, the following equations can be written:

$$\rho_g=\rho_w A/(B-C) \qquad (5)$$

where ρ_g is the compact density and ρ_w is water density.

The percentage of open porosity (%P) can be calculated from:

$V_{porosity}/V_{green}=[(B-A)/\rho_w]/[\rho_w/(B-C)])$

$$\%P=(B-A)/(B-C)\cdot 100\% \qquad (6)$$

1.5.2 Mercury Intrusion Porosimetry

In mercury porosimetry measurements, the pore size distribution and density of a material are determined. The pore sizes that can be determined range from a few nanometers to hundreds of microns. During the measurement, pressure is used to force mercury into the open pores of the material.[19] Mercury does not wet most substances and will not penetrate pores by capillary action, thus an external pressure inversely proportional to the pore diameter is required for infiltration. For simplicity, pores are assumed to be in the form of aligned cylinders. When mercury is in contact with a pore opening, with a circular cross-section, the surface energy of the mercury acts along the circle of contact (see Figure 1.9). Thus the force with which mercury resists entering the pore is equal to:

$$F=\pi D_p \gamma \cos\theta \qquad (7)$$

where D_p is pore diameter, γ is the surface energy and θ is the contact angle.

The force due to an externally applied pressure acts over the area of the circle of contact and is expressed by:

$$F=\pi D_p^2 P/4 \qquad (8)$$

where P is the applied pressure. At equilibrium, the opposing forces are equal:

$$\pi D_p^2 P/4 = \pi D_p \gamma \cos\theta \qquad (9)$$

After simplification, the pore diameter can be easily calculated using the following equation:

$$D_p=-4\gamma\cos\theta/P \qquad (10)$$

Finally, the injected volume of mercury as a function of pressure indicates the amount of pores of a certain diameter.[40]

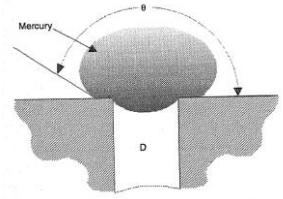

Figure 1.9: Mercury in contact with a porous material.[40]

2 Research Objectives

The aim of this study is to develop an experimental approach for the characterization of water-based high solid-load (Mg-spinel) suspensions by cryo-SEM, augmented by conventional rheological characterization techniques. The Mg-spinel system was chosen as a test case. This work demonstrates that cryo-SEM can provide better understanding of the microstructure of suspensions as a function of composition and solid loading, at solid-loading contents for which conventional particle size measurement tools are not applicable. A secondary goal was to characterize diluted suspensions, and to evaluate the size distribution of primary particles.

3 Experimental Methods

3.1 Preparation of Suspensions

High purity (99.9%) $MgAl_2O_4$ spinel powder (Baikowski, France) with a nominal powder size distribution (provided by the manufacturer) of d_{50}=0.21μm was used as a starting material. De-ionized water (18MΩ) was used for the suspension. Ammonium polyacrylate (R.T. Vanderbilt, Connecticut, US) was used as a dispersant (5wt.% of the powder). Ammonia and nitric acid were used to adjust the pH of the suspensions. Alumina milling balls (10mm diameter, Tosoh, Japan) were used for de-agglomeration by ball-milling for 24 hours at a suspension/ball ratio of 1 to 6 (by weight). Impurities in the powder were identified using induced coupled plasma spectroscopy (ICP), and found to be close to those defined by the powder manufacturer (see Table 3). The specific surface area of the powder was determined by the BET method using nitrogen adsorption (Micromeritics Instrument Corporation, GA, US).

Element	Concentration [ppm]
Na	10
Ca	5
Fe	10
Si	20

Table 3: Impurities in the initial spinel powder, as determined from ICP.

3.2 Suspension Characterization Methods

3.2.1 Particle Size Distribution

Particle size distributions of the raw powder and as-milled suspensions were measured using static light scattering (SLS, Mastersizer, Malvern Instruments). The measured suspensions were diluted to 500-5000ppm.

3.2.2 Zeta Potential Measurements

Zeta potential measurements were acquired using a NiComp380 ZLS Zeta Potential Analyzer (Particle Sizing Systems, Santa Barbara). The measured suspensions were diluted to ~150ppm. The pH was adjusted using 0.1M nitric acid

(HNO_3) and 0.1M ammonium hydroxide (NH_4OH). Concentrated acid and base solutions were also used, to avoid excessive dilution.

3.2.3 Rheological Measurements

The rheological properties of a fluid provide information concerning its behavior under shear stress exerted at certain intensities and rates, keeping in mind that colloids are usually non-Newtonian systems. Viscosity measurements were performed using a rotary viscometer (Model LVDV-II, Brookfield), based on ASTM standard E-112.[41] Measurements were taken for time durations of minutes to hours, under constant shear rates, and also under increasing and decreasing shear rates. Some of the measurements were performed after "aging", where the spindle was allowed to rest for a given time while submerged in the suspension, before rotating it.

3.2.4 Cryo-SEM

The fundamental concept of cryo-SEM as applied to this study was to rapidly cool the suspension, followed by high resolution SEM conducted at cryogenic temperatures, such that the morphology of the spinel particles within the microstructure of the suspension could be investigated. While cooling the aqueous ceramic suspension, ice crystal formation can cause distortion of the sample morphology due to volume changes which occur upon crystallization. To avoid the formation of crystalline ice, the suspension must be rapidly cooled.

Sample preparation for cryo-SEM took place under controlled environmental conditions of temperature and humidity within a dedicated chamber (see Figure 3.1). Special “plunging tweezers” were inserted into the controlled atmosphere chamber for handling the samples, including rapid cooling.[39]

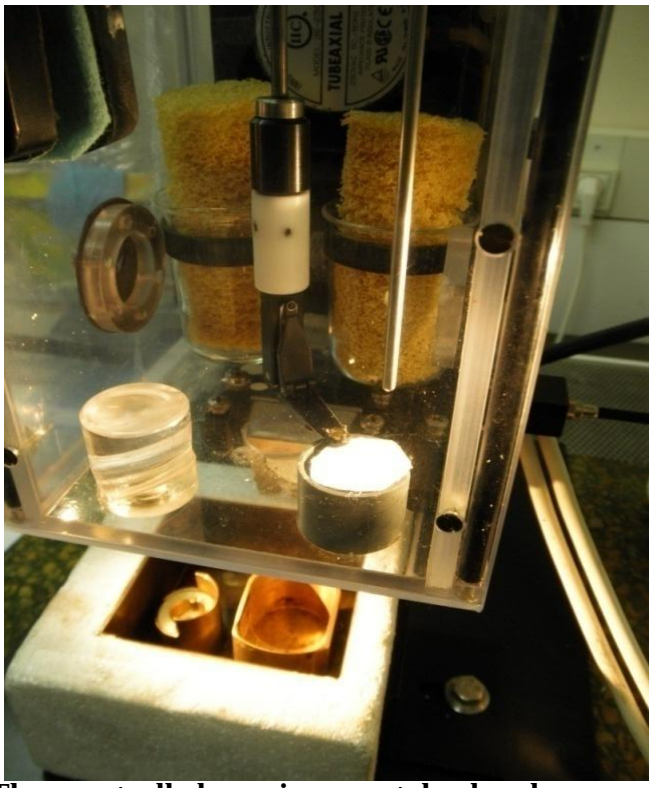

Figure 3.1: The controlled environmental chamber used for preparing specimens.

As shown in Figure 3.2, a sample cell was assembled inside the chamber, based on a gold planchette placed inside the cavity of the plunging tweezers and a ~5µl droplet of the investigated suspension was placed on the planchette, followed by a second gold planchette to close the sample. A copper grid (200mesh) was also placed between the two gold planchettes, to facilitate fracturing the droplet after vitrification.

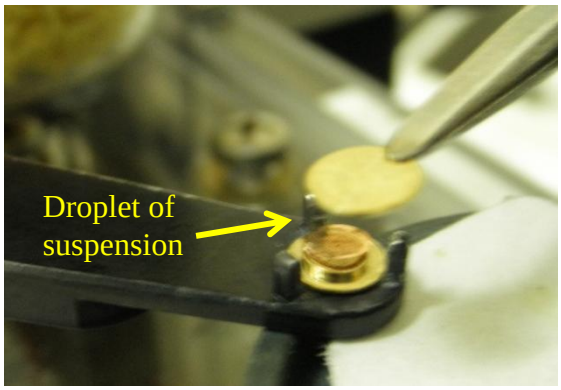

Figure 3.2: Photograph of the "Sandwich" assembly, where a 5µl droplet of suspension is placed between two gold planchettes.

During the vitrification process, the tweezers holding the sample were rapidly plunged into a cup filled with cryogen. The chosen cryogen, liquid ethane, was pre-cooled to its freezing point by cooling using liquid nitrogen. The freezing point of ethane (-183°C) is higher than the boiling point of liquid nitrogen (-196°C). As such, gaseous ethane was condensed in a container surrounded by a bath of liquid nitrogen (as shown in Figure 3.3). Then the sample was quickly plunged into the liquid ethane before the ethane froze. This process is designed to prevent distortion of the suspension's microstructure by volume changes due to crystalline ice formation, such that subsequent SEM micrographs reflect the true microstructure of the original suspension.[42] After thermal fixation the specimen was stored in liquid nitrogen.

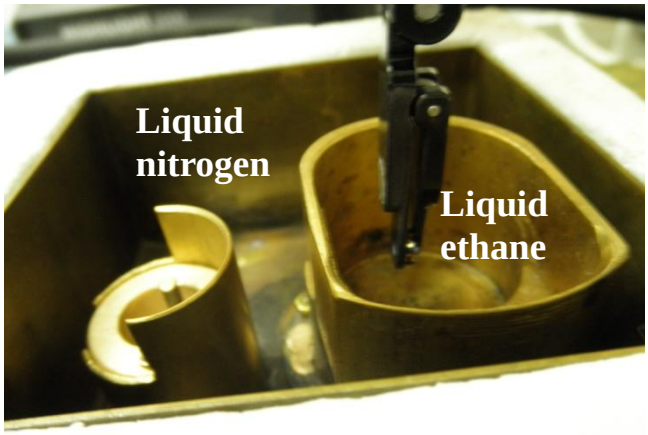

Figure 3.3: Photograph of the liquid ethane bath and sample used for vitrification.

The vitrified specimen was then inserted into a cryo-SEM specimen holder (see Figure 3.4) under liquid nitrogen, and transferred to a BAF-060 system (BAL-TEC, AG, Liechtenstein) for preparation of the sample surface prior to SEM.

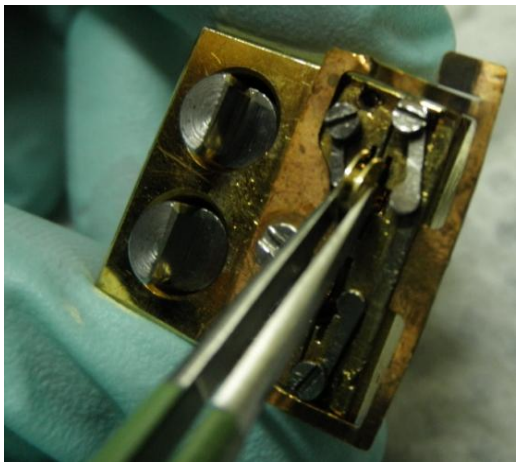

Figure 3.4: Photograph of the "Sandwich" being inserted into the sample holder, under liquid nitrogen (not seen in the picture)

The BAF-060 system was maintained at a vacuum of 0.001 Pa prior to introduction of the sample, and pre-cooled to approximately -170°C. The specimen was then fractured in-situ (see Figure 3.5), and thermally etched. Etching was conducted by raising the temperature to -104°C to sublime water and to expose the morphology of the non-vaporized materials (ceramic particles and organic materials). The sublimation time was optimized to expose the floc microstructures and retain their integrity.[43]

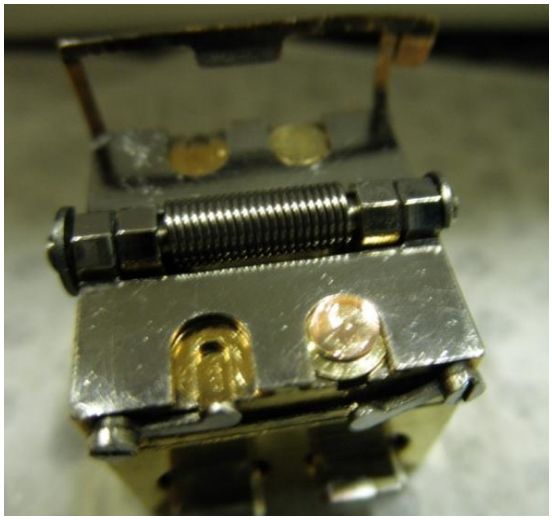

Figure 3.5: Photograph of the sample holder which upon opening fractures the vitrified sample.

Since the ceramic suspensions are electrically insulating, the vitrified specimens were coated with a thin film of conductive material (platinum and carbon) in the BAF-060 system, to avoid charging by the SEM electron beam. After coating, the specimens were transferred using a transfer shuttle (VCT-100, Leica Microsystems, Vienna, Austria), to the pre-cooled cryo-stage in a dedicated cryogenic high resolution SEM (Ultra Plus HRSEM, Zeiss), equipped with a Schottky field-emission electron source. Micrographs were acquired at working distances of 2.8 to 5mm, using both secondary electrons (in-lens and Everhart-Thornley detectors) and backscattered electrons, at a relatively low accelerating voltage of 3-3.5kV. This range is assumed to minimize charging, because the number of electrons hitting the specimen is equal to the number of electrons generated from the hit. That range was chosen, based on the equivalent voltage range for alumina (which is similar to spinel in composition and density). Issman and Talmon describe the details of this procedure.[39]

3.3 Green Compact Characterization

As-milled spinel suspensions were cast on porous alumina molds (33% porosity) via two different procedures, to produce two kinds of green compacts (see Figure 3.6):

a. The alumina mold was dried and started to absorb water from the suspension immediately upon casting, to form a green compact of the as-milled suspension.

b. The alumina mold was immersed in water, to delay water absorption. The as-milled suspension was allowed to flocculate for 2 to 3 days, and then the mold was taken out of the water and was allowed to dry. This procedure resulted in a green compact formed of an *aged* suspension. 10-12 spinel green compacts were cast by each procedure (see Figure 3.7).

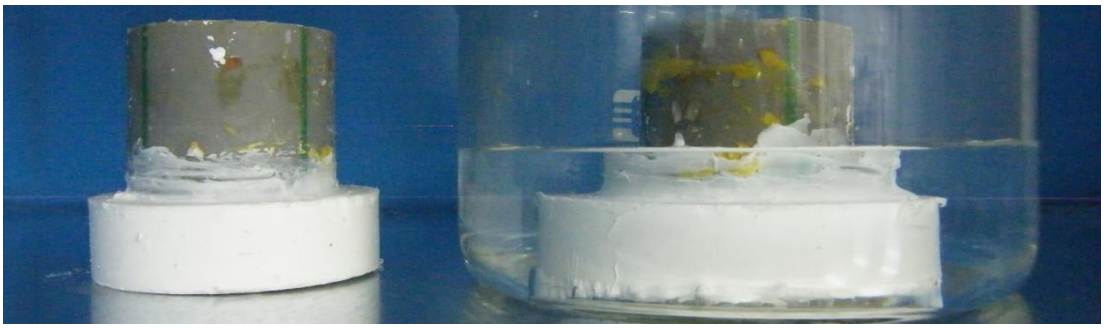

Figure 3.6: Photograph of the spinel suspension cast on: a) a dry mold; and b) a wet mold.

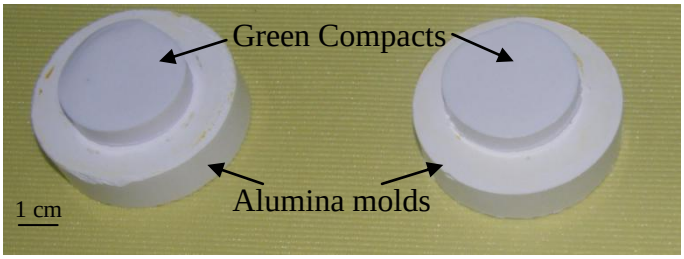

Figure 3.7: Photograph of the spinel green compacts on porous alumina molds.

These two procedures were expected to result in green compacts with different green densities and microstructures: the microstructure expected for a flocculated suspension is less homogeneous than the one for the as-milled suspension. The green density and pore size distribution were measured for these samples.

3.3.1 Green Density from Archimedes' Principle

The density of green compact was measured after firing (heating to 900°C for 2 hours, where necks are formed between particles without any increase in density), by the following: the dried and fired specimens were weighed (A in equation number (6)). The specimens were then immersed in hot water for 5 hours, and allowed to cool for 24 hours. Measurement of the wet specimen weight (B) was done after water absorption and cooling, and C was measured when the wet specimen was weighed while immersed in water.

3.3.2 Mercury Intrusion Porosimetry

Porosity measurements were performed using a Macropore 120 Porosimeter 2000 (Carlo Erba Instr., Italy). Two specimens were measured, one from each group (a and b). Specimens were loaded in a sealed cup and evacuated to remove air and moisture. The cup was backfilled with mercury. As the pressure increased, mercury infiltrated into the specimen's pores, beginning with those of larger diameters. The green compact density was determined from:

$$\rho_g = \frac{1}{(V_T - V_I)+(1/\rho)} \qquad (11)$$

where V_T is the total cumulative pore volume, V_I is the volume backfilled with mercury under low pressure (not attributed by pores) and ρ is the spinel theoretical density.

4 Results

4.1 Powder Characterization

According to BET measurements, the specific surface area (S_{BET}) of the un-milled (raw) powder is $30m^2/gr$. As mentioned before, particles with such large surface areas tend to agglomerate and flocculate. Assuming the particles are uniform spheres, their diameter (d) can be estimated to be ~55nm, using a $MgAl_2O_4$ theoretical density of ρ=3.58gr/cm^3 and $d_{(nm)}=6/(\rho \cdot 10^3 \cdot S_{BET})$. However, static laser scattering (SLS) measurements of the raw powder present a wide particle size distribution with two main peaks around 0.4 and 2.2μm (see Figure 4.1).

SLS measurements of the milled suspension indicate that the ball-milling process reduces agglomeration, by breaking soft agglomerates. The residual hard agglomerates after complete ball-milling have an average size of 170nm, distributed between 0.08 and 0.5μm.

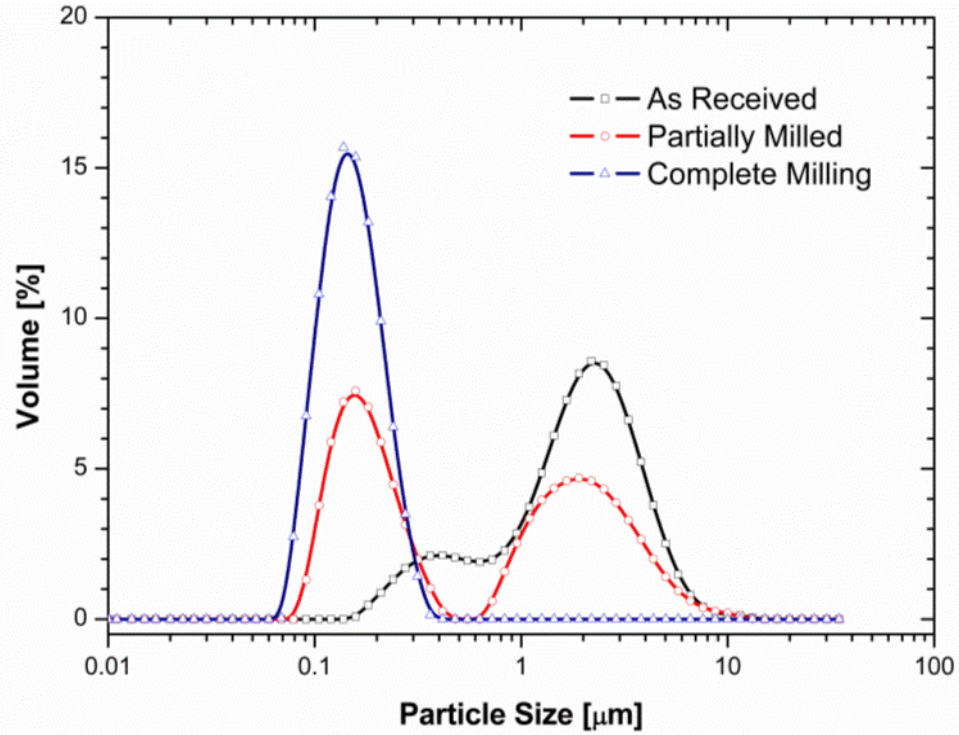

Figure 4.1: Particle size distribution of the spinel powders, after different times of ball-milling, acquired from static laser scattering (SLS).

4.2 Zeta Potential

Zeta potential measurements were used to estimate the stability of suspensions in terms of electrical repulsion.[44] A dilute (150 ppm) spinel *slurry* (powder and water) was prepared to find the IEP for the powder, where the pH value results in zero net charge density on the surface of the particles.[22] The pH of the slurry was adjusted, while keeping a constant ionic concentration. As presented in Figure 4.2, as the pH rises, the zeta potential decreases. The IEP of the powder particles in water was found to be 11.8. This value agrees with values found from other studies.[45,46]

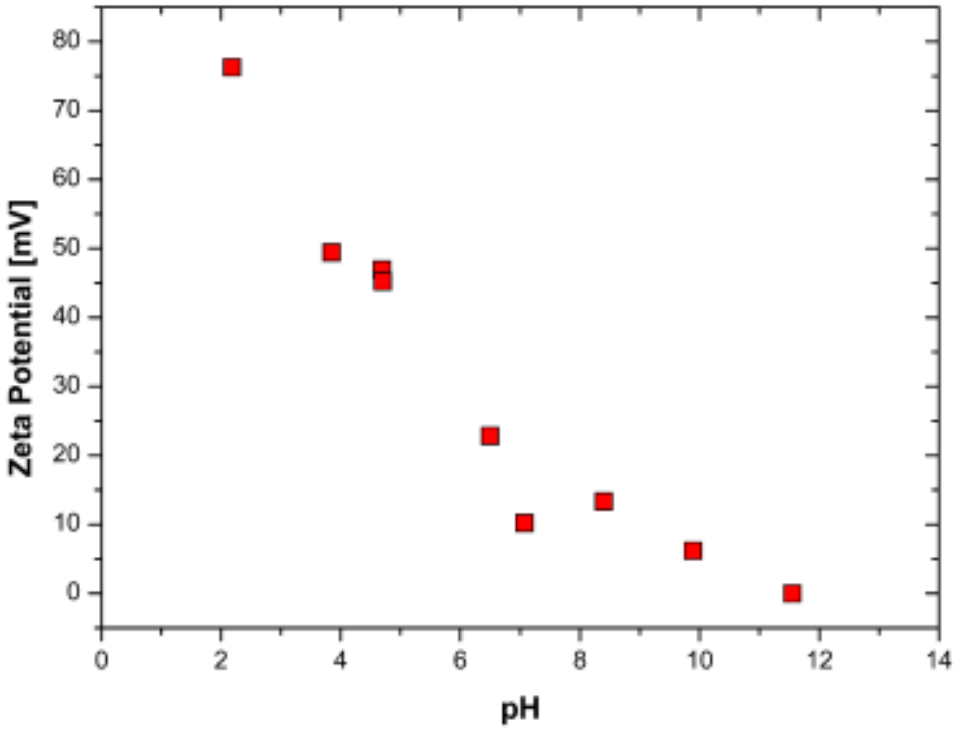

Figure 4.2: Zeta potential of spinel powder in water (~150ppm) at different pH levels. The spinel IEP is at pH~11.8.

The zeta potential of the investigated (diluted) *suspension* was measured at different levels of pH to find its IEP. It was found that the isoelectric point shifted to pH~3.3 upon addition of the polyacrylate dispersant (see Figure 4.3).

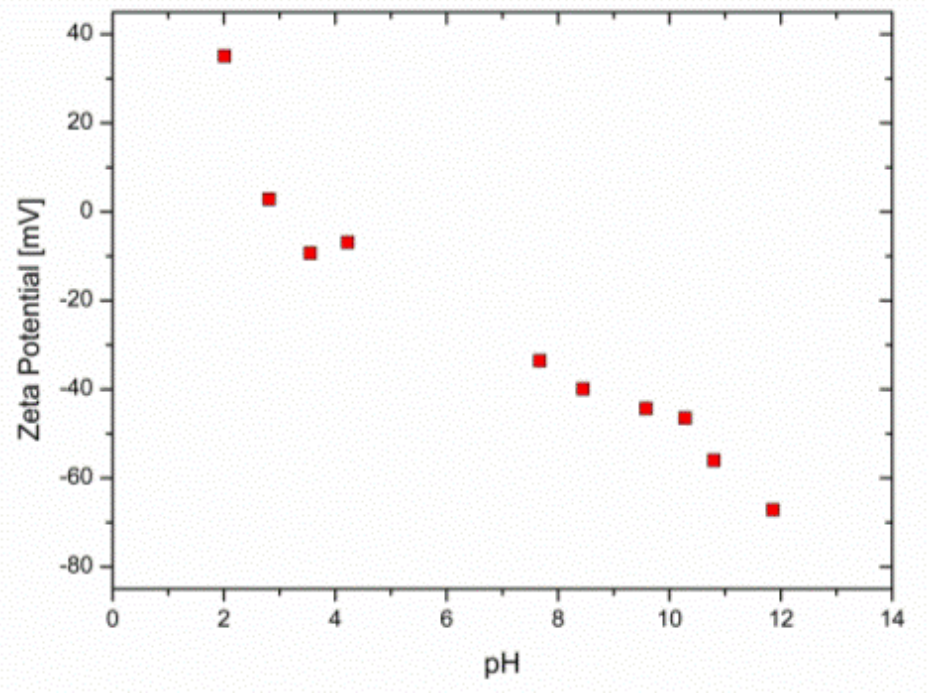

Figure 4.3: Zeta potential of the investigated spinel suspension at different pH levels.

4.3 Rheological Measurements

Flocculation is defined as nucleation and growth of particle clusters.[22] Since flocculation increases the viscosity, a non-flocculated suspension will have a lower viscosity than a flocculated one. The viscosity was measured for a 60 wt.% suspension (immediately after milling), at 26°C using the Broookfield spindle number 3, while increasing and decreasing the shear rate (see Figure 4.4).

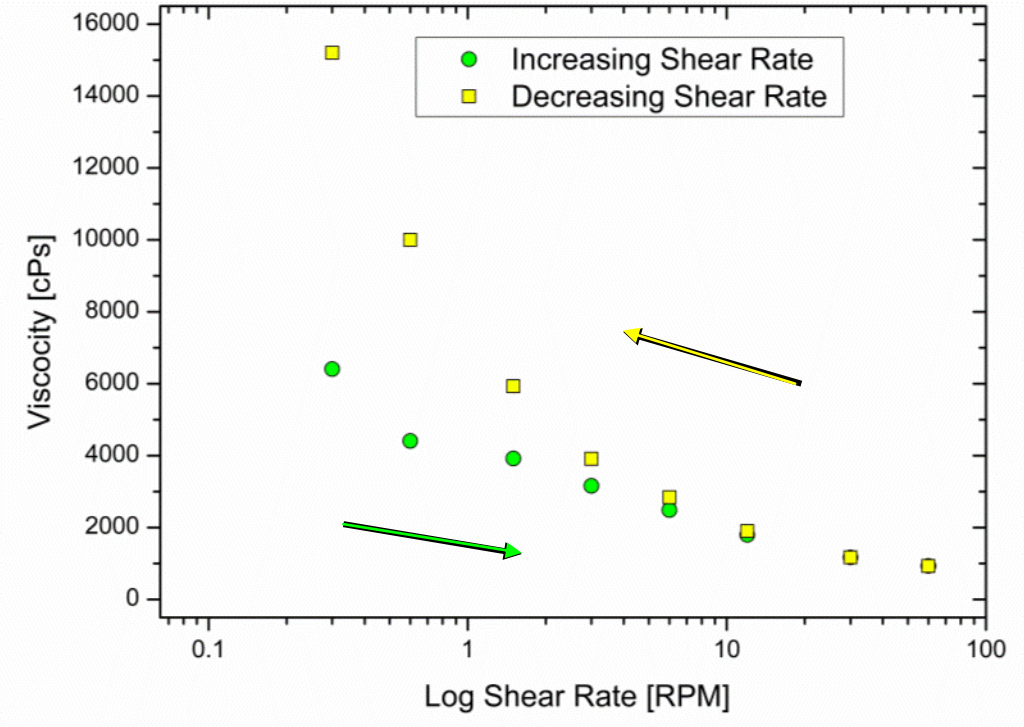

Figure 4.4: The viscosity vs. shear rate for a 60 wt.% spinel suspension.

An inverse relation was found between viscosity and shear rate, where the viscosity decreased as the shear rate was increased. This phenomenon is referred to as shear-thinning (i.e. pseudo-plastic) behavior, which is well known in colloidal systems.[12]

The viscosity of the "fresh" (as-milled) suspension was measured as a function of time under a constant rate of shear (Brookfield spindle number 3 at 60 rpm). "Ageing" of the suspension was investigated by vigorously shaking a "fresh" suspension for at least 10 minutes, followed by resting the suspension for 20 minutes (the aging period). Afterwards, its viscosity was measured again, as a function of time under a constant rate of shear. The aged suspension is significantly more viscous than the suspension immediately after ball-milling. Both fresh and aged suspensions showed decreasing and then increasing viscosity with time under a constant shear rate (see Figure 4.5).

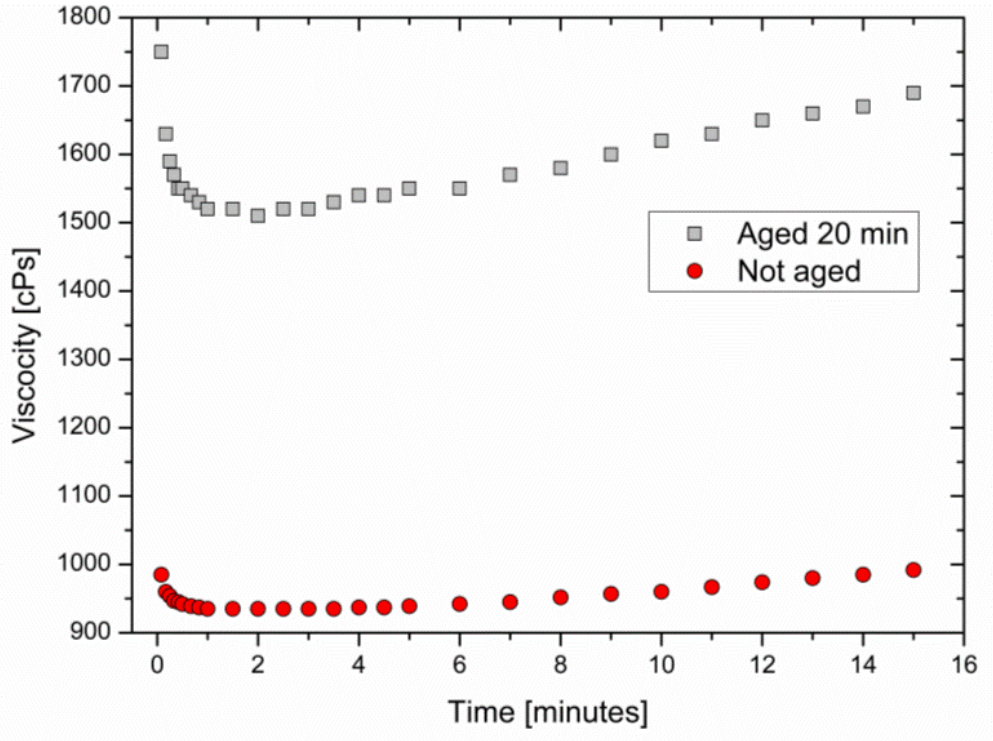

Figure 4.5: Viscosity versus time for a 60 wt.% spinel suspension, measured using Brookfield spindle number 3 at 60 rpm.

4.4 Cryo-SEM

Specimens of the investigated suspensions were prepared according to the procedure described above. A suspension of 60 wt.% solid-loading was ball-milled, after adjusting the pH to higher than 10 (to obtain a good dispersion). The ball-milled suspension was shaken vigorously immediately before preparing the sample. Figure 4.6 shows the presence of both agglomerated and flocculated particles. Flocs are indicated by white circles, and residual agglomerates by red circles. The filaments indicated by arrows are bundles of the polymeric dispersant.

The suspension was then aged for half an hour, and another sample was prepared. Figure 4.7 demonstrates that the aged suspension is heavily flocculated.

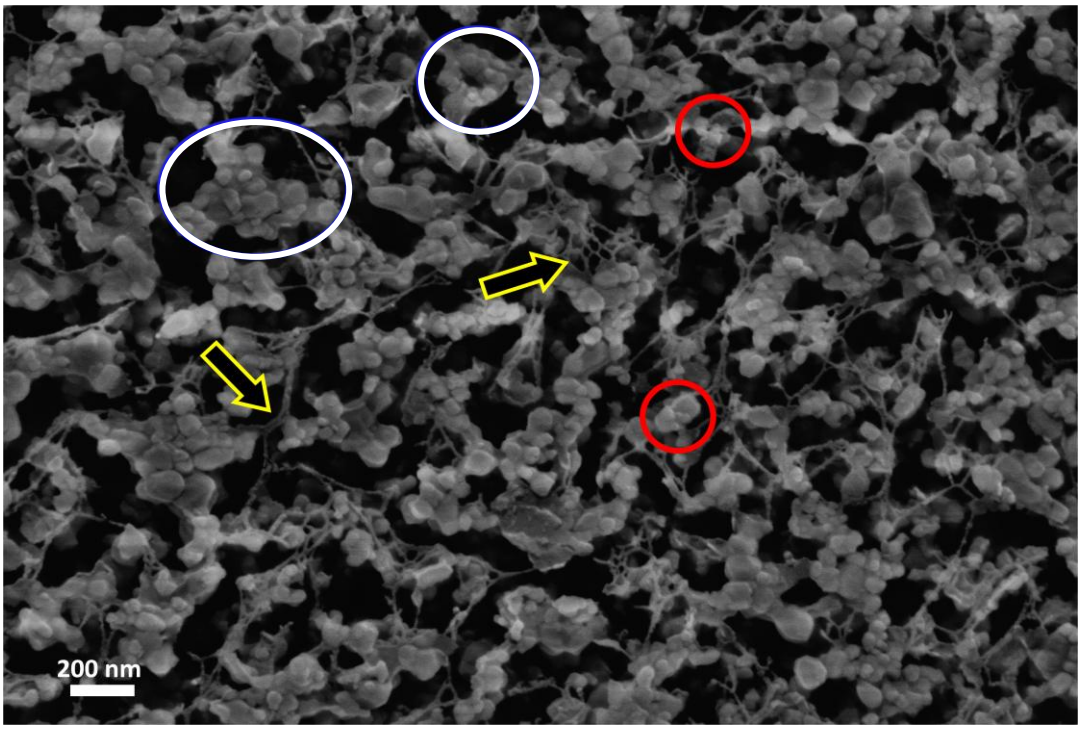

Figure 4.6: Secondary electron cryo-HRSEM micrograph, based on a combined signal from in-lens and conventional secondary electron detectors, of a 60 wt.% spinel suspension without aging.

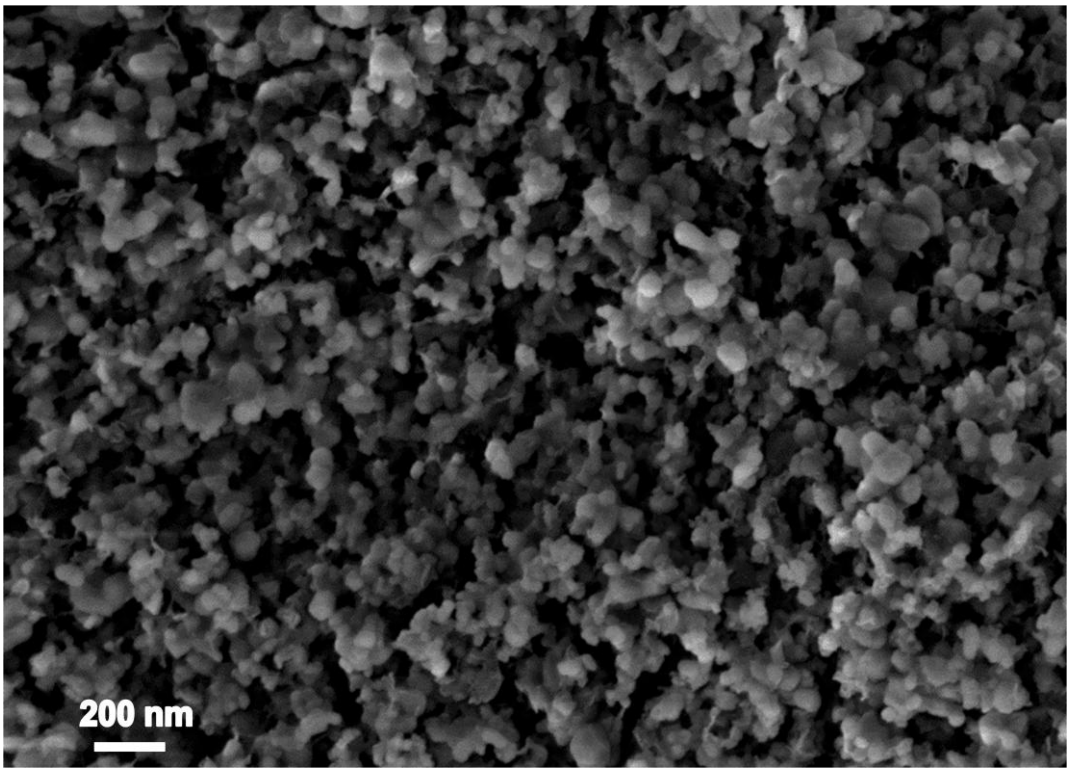

Figure 4.7: Secondary electron cryo-HRSEM micrograph, based on a combined signal from in-lens and conventional secondary electron detectors, of a 60 wt.% spinel suspension after 0.5 hour aging.

The 60wt.% suspension was diluted to 0.6wt.%, and another specimen was prepared for cryo-SEM. As shown in Figure 4.8, the diluted suspension is consisted of particles of approximately 100-200nm in diameter, and a polymeric solution matrix.

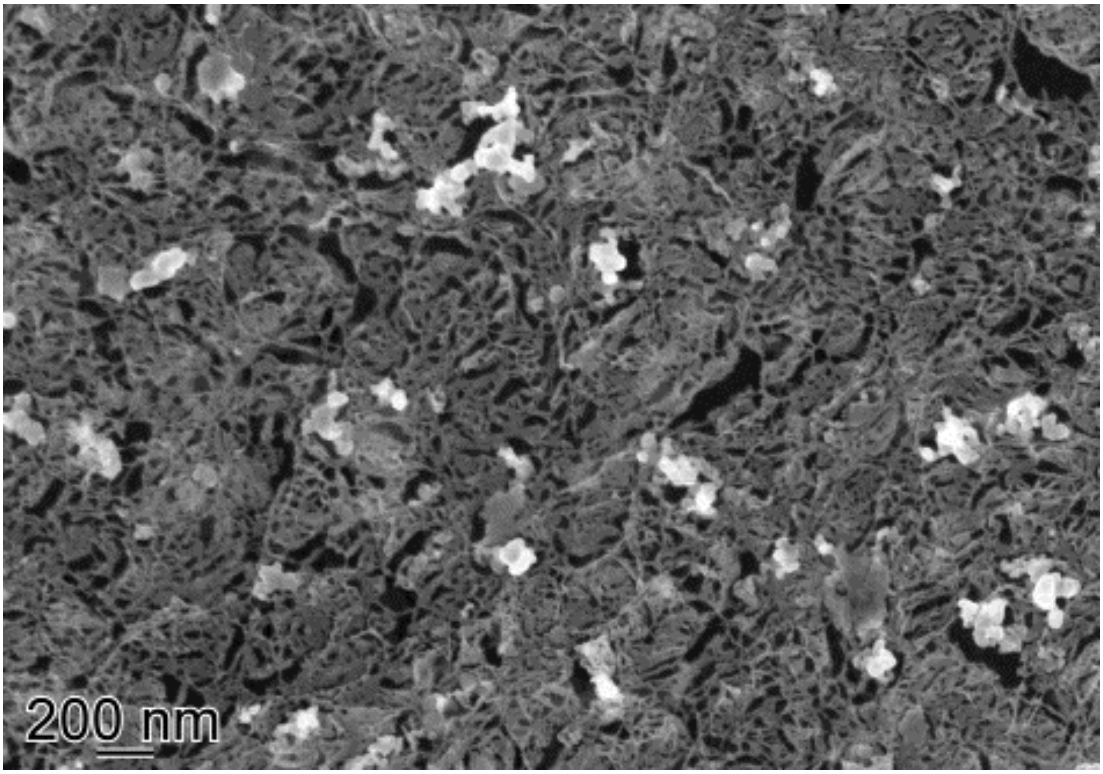

Figure 4.8: Secondary electron cryo-HRSEM micrograph, based on a combined signal from in-lens and conventional secondary electron detectors, of a 0.6 wt.% suspension diluted from the original 60 wt.% suspension.

Using image analysis software (ImageJ), the particles in the micrographs of the diluted suspension (Figure 4.8) were differentiated from the background, and their cross-sectional area was measured (Figure 4.9 and Figure 4.10). The diameter of the elementary particles was determined from the cross-sectional area, assuming a spherical shape. The particles diameter-distribution is presented in Figure 4.10. Most of the elementary particles are between 25 to 55 nanometers in diameter.

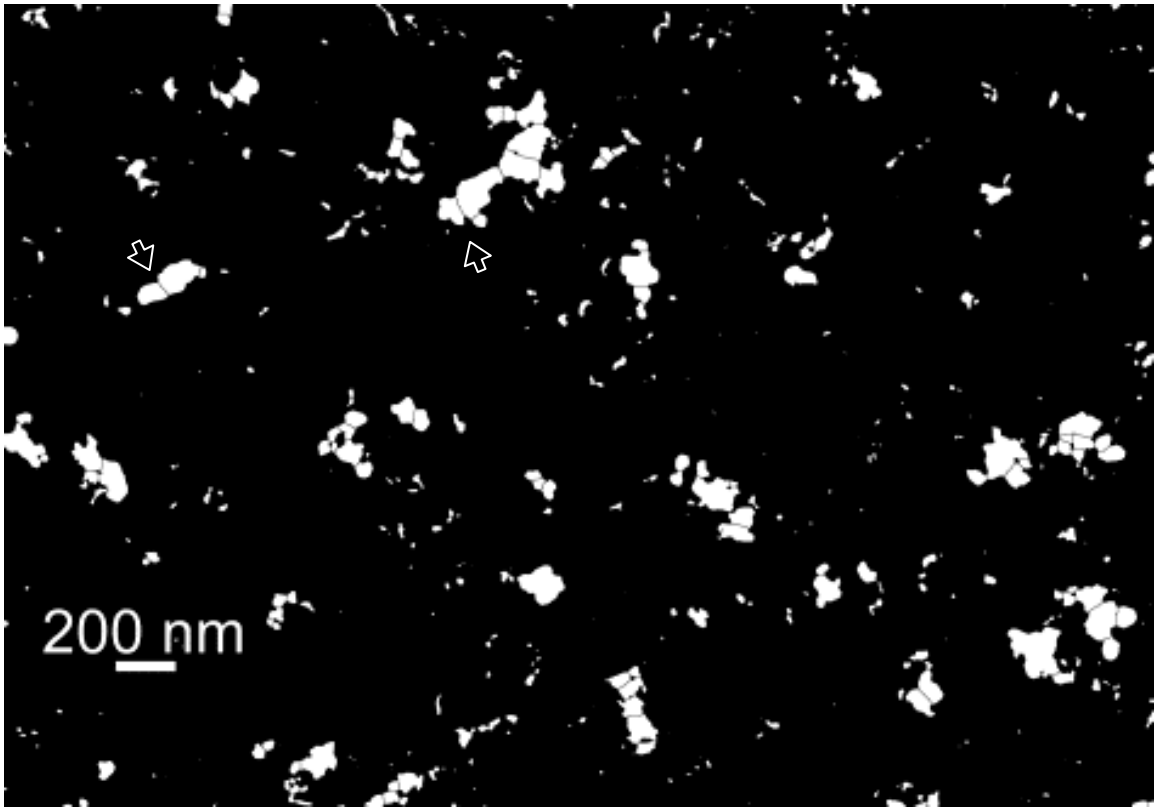

Figure 4.9: The micrograph in Figure 4.8 after processing using the ImageJ software. The thin lines, indicated by arrows, are the boundaries between elementary particles in the suspension.

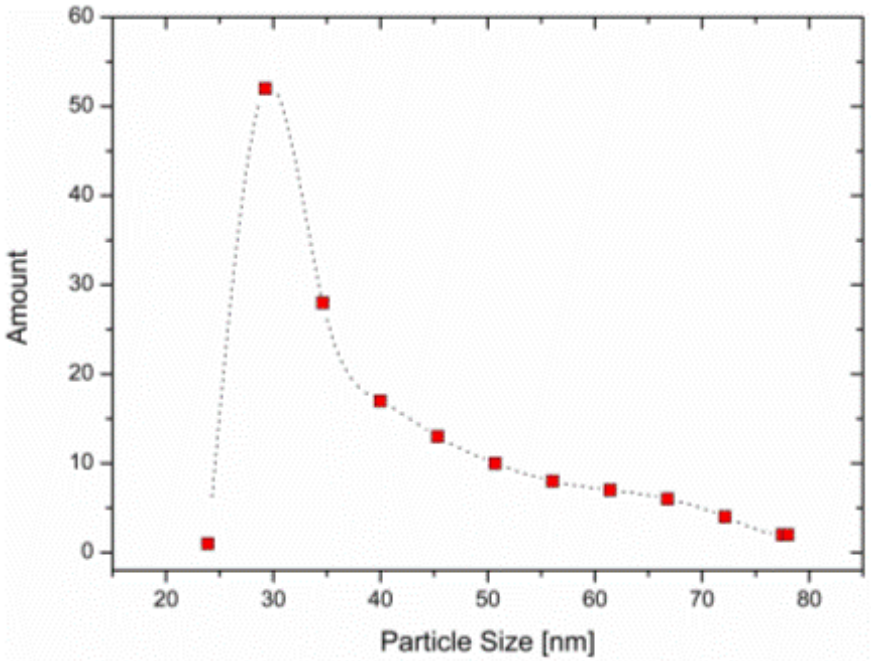

Figure 4.10: Results from image analysis after processing. Most of the elementary particles are between 25 to 55 nm in diameter.

4.5 Green Compact Density and Porosity

The results acquired from porosimetry are presented in Figure 4.11 and Figure 4.12. As illustrated in Figure 4.11, both the specimen cast into a dry mold and the one cast into a wet mold have a similar pore size distribution. The specimen, cast into a wet mold presents a minor shift to higher pore diameters, but this is probably a negligible difference. Most of the pores are between 30-55nm in diameter.

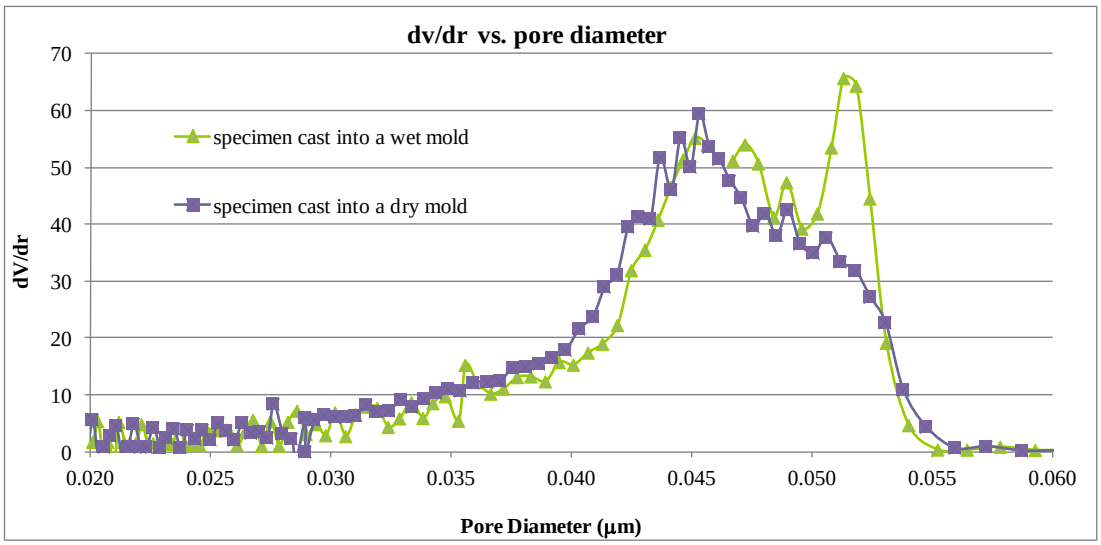

Figure 4.11: Incremental volume of pores versus pore diameter.

When addressing the cumulative volume results (Figure 4.12), the graphs are also similar and the difference is inconclusive. The inset in Figure 4.12 focuses on the largest pore diameters, where differences between the graphs are clearer. The green compact cast from the as-milled suspension presents a higher fraction of large porosity: 0.1 of its porosity is larger than 0.1 micron, whereas for the compact cast from aged suspension, the largest pore size is smaller.

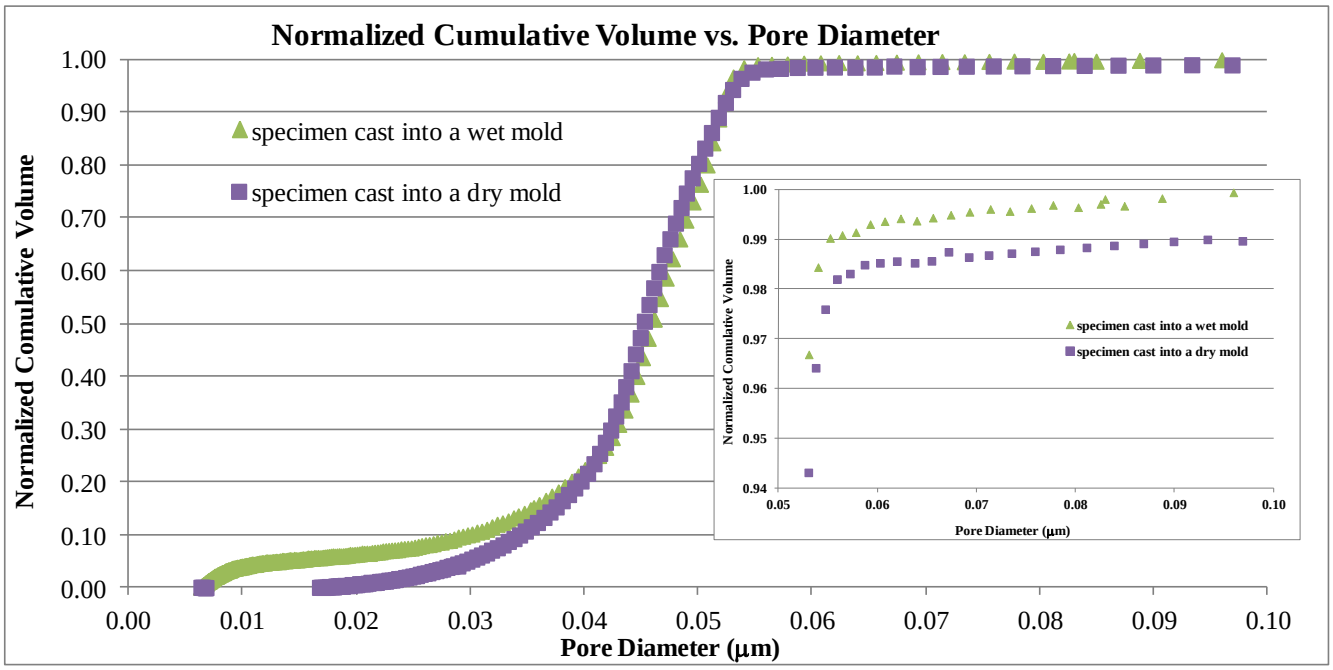

Figure 4.12: Normalized cumulative volume of pores versus pore diameter.

The percentage of theoretical density (%TD) was determined. The density measured by the Archimedes method and by porosimetry tests were divided by the theoretical density of spinel. As inferred from Table 4, the results are similar for both methods and for both casting procedures (compacts created by as-milled and aged suspensions).

Green compact casted from:	%TD measured by Archimedes method	%TD measured by porosimetry test
As-milled suspension	43.2%	44.9%
Aged suspension	43.1%	42.9%

Table 4: Green compact average density, calculated by Archimedes method and by porosimetry results, for 10-12 specimens casted from as-milled and aged suspensions.

5 Discussion

The average particle size calculated from specific surface area measurement, compared with the particle size distribution obtained by SLS, indicate that the un-milled powder is agglomerated. The average diameter calculated from the specific surface area is that of the elementary particle, while the size determined from static laser scattering indicates the diameter of the agglomerates (Figure 4.1).

The ball-milling process promotes partial de-agglomeration. The narrow size distribution obtained after 24hr milling indicates that this is the optimal milling duration for this specific powder. Milling times of less than 24hr are insufficient, and may lead to a non-homogeneous porous structure of the green-compact, and therefore residual porosity in the sintered compact. After ball-milling, the hard agglomerates remain. As presented in the results obtained by SLS for the suspension after complete milling, the elementary particles of the powder form hard agglomerates of about 100 to 200nm in diameter (the peak at 170nm). These agglomerates can also be detected by cryo-SEM imaging of the diluted suspension, from which their size is between 100 and 200nm (Figure 4.8). When diluted, the suspension presents a well-dispersed, non-flocculated microstructure, as expected from suspensions at low solid-loading, unlike the original, high solid-load suspension (Figure 4.6). The polymer, presumably with some water adsorbed to it, forms the matrix visible in the background, perhaps as a result of local freezing, and sublimation.

Image analysis results of the diluted suspension cryo-SEM micrograph show that the elementary particles (composing the hard agglomerates) are distributed between 25 and 80nm in diameter, while most are between 25 and 55nm in diameter. When calculating the diameter-based on BET measurements (specific surface area), it is assumed that all the particles are of the same diameter, resulting in an average size of 55nm. This assumption is misleading, and the calculated size represents a variety of diameter distributions.

Considering the high zeta potential values at alkaline pH, a stable dispersion achieved for low solid-loading suspensions is foreseen. Side groups along the polymeric chain dissociate at high pH values, generate negatively charged sites,

while the powder, as confirmed using zeta potential measurements, presents a positive net surface charge density at pH values lower than the IEP (11.8). The positively charged sites on the powder particles function as anchoring sites for the polymer. The abundant negatively charged groups on the polymer cause the negative values of zeta potential. They repel each other and facilitate the dispersion. In addition, the polymer attached to the particle surface impedes particle contact, thus facilitates steric hindrance, avoiding the primary minimum in the pair potential curve.[47] According to DLVO theory, a high absolute value of zeta potential is necessary to prepare stable aqueous suspensions.[12] A sufficient repulsive force between particles is required to overcome the attractive van der Waals interactions, which tend to hold the particles together (forming aggregation and flocculation).[9] Vallar et al. stated that absolute values of zeta potential higher than 50mV can serve to predict stable suspensions.[23] Following that, for this research work, basic values of pH higher than pH=10 should form a good dispersion.

However, while the determined IEP is not affected by slurry concentration, zeta potential measurements (performed on dilute suspensions) at most values of pH do not necessarily represent the pH required to disperse non-dilute slurries (used for casting). For suspensions with high solid-loading, van der Waals (vdW) forces between particles are more significant in defining the stability of the suspension, because of the shorter mean distance between particles. Moreover, for these concentrations of particles in suspension, double-layers or adsorbed polymer layers can interpenetrate, thus leading to coagulation, particularly after aging.[47] The measuring method used in this research employs light for the characterization. Light is scattered from the particles (when they move under an electric field), and in order to reach the detector the sample must be transparent. Therefore, the original suspension was diluted and corresponding zeta potential measurements for this (high solid-load) suspension were not possible. Although the high value of zeta potential measured for a dilute suspension can indicate that it is dispersed, a non-dilute suspension may become flocculated due to the dominant vdW attraction forces.[48,49] It should be noted that the zeta potential for high solid-load suspensions can be measured using electro-acoustic approaches, but that method is beyond the scope of the current research.[50]

The rheological behavior of the original suspension indicates that it flocculates, while the aggregates (flocs) present in the suspension increase the suspension viscosity.[51] The suspension behaves as a shear-thinning (i.e. pseudo-plastic) system, as low shear rates allow flocculation, while higher shear rates break flocs, and reduce the viscosity. In other words, the decrease in viscosity with increasing shear rate can be explained by the increased rupture of links between flocs with increasing shear rate, providing easier flow of the liquid.[23,52] The increased viscosity for the same values of shear rate, at later stages of the experiment, can be explained by flocculation, which takes place even during the experiment, although the suspension is stirred.

For both suspensions (as-milled and aged), the viscosity initially decreases with time under constant shear, as expected from a thixotropic system. Later on, the trend reverses, and the viscosity rises. Although the viscosity eventually rises, the aged suspension can be referred to as thixotropic (an apparent viscosity that decreases with time under shear).[12] The decreased and then increased viscosity may indicate that flocs are first broken and then re-formed. When the suspension is at rest (during aging), the particles move in Brownian motion, and collide. When the suspension is stirred during the measurement, the spindle facilitates laminar flow. Particles in a uniform laminar shear-flow collide because of their relative motion. A particle closer to the rotating spindle, moving at a higher velocity, overtakes and collides with a slower moving particle, farther from the spindle. Friedlander et al. suggested that the Brownian motion (when the suspension is at rest, during the aging period) and laminar shear (when the suspension is stirred) both contribute to flocculation and coagulation, but at higher shear rates the contribution of the Brownian motion to coagulation may be neglected.[53] Although high shear rates are assumed to breakup large flocs, it is expected that the shear stress will increase the collision frequency, and hence quickly create large floc aggregates. In addition, higher shear rate may form denser flocs.[54]

From these results it may be concluded that aging promotes flocculation of the suspended particles, as the attractive forces between particles increase with time. To separate the flocs, a higher shear stress is required. Hence, the viscosity of the aged suspension is initially higher than that of the as-milled suspension.

A viscosity rise during the measurement indicates that either the flocs are denser (harder to breakup), or that there are more flocs (the flocculation rate increases). Therefore, the flocs formed by laminar shear are either stronger or more quickly formed than the flocs formed due to Brownian motion at rest. It should be noted that vigorous stirring (turbulent flow) applied to the aged suspension reduced its viscosity to the initial (non-aged) value. Figure 4.6 of the fresh suspension, demonstrates that the as-milled suspension is weakly flocculated. The hard agglomerates that remain after ball-milling, assemble into porous flocs. The regions with dark contrast between the particles are the holes left after water sublimation. The filaments indicated by arrows are bundles of the polymeric dispersant, formed during sublimation before observation, and may imply either a redundant or deficient amount of dispersant in the suspension. The excessive amount of polymer causes "bridging", or links between the particles, which holds them together and promotes flocculation.[18,22] Conversely, when the amount of dispersant is too low, particle coverage by adsorption of the polymer is incomplete, and may also provide a driving force for particles to cluster.[22] The surface chemistry of the suspended particles can also affect flocculation. Ganesh et al. suggested that flocculation and coagulation of Mg-spinel aqueous suspensions at solid-loadings higher than 30vol.% (~60wt.%) are initially caused by powder hydrolysis.[9,25] Aging is shown here to promote flocculation. Qualitative differences in the microstructure between the weakly flocculated suspension and the (aged) strongly flocculated suspension can be observed. The weakly flocculated suspension shows a homogeneous structure of separated flocs, whereas the microstructure of the strongly flocculated suspension is inhomogeneous, and is characterized by voids between areas of densely packed aggregates. The seemingly denser structure of the aged suspension is attributed to the multiple levels of particles.

It is commonly assumed that a good dispersion of particles gives an optimum packing state (higher green density), which influences the sinterability of the ceramic body, and hence the properties of the final product.[55] Hence, the green structure was assumed to be influenced by the flocculation state of the suspension it was cast from. Mercury porosimetry measurements indicate that both of the specimens have a similar pore size distribution, although it is expected that the green-compact made

from an aged suspension would have larger pores (due to the more flocculated and less homogeneous microstructure of that suspension). The similar pore size distributions, and the tail of large porosity in the green-compact cast from the as-milled suspension, may be explained by its drying process. The drying process starts immediately when the suspension wets the porous mold. Hence, the layer close to the porous mold is dried before it flocculates. Thus the microstructure obtained in the first layer is of larger pores, as presented in the magnified tail of porosity (small graph) of Figure 4.12. After the first drying stage, the pores in the mold are saturated with water, and water from the suspension is absorbed more slowly. When the drying process slows down, the suspension flocculates. Therefore, most of the green-compact dries when its microstructure is already flocculated and fixed. The drying process of the compact cast from the aged suspension is similar. It is delayed to the point when the cast suspension is already flocculated. As opposed to the compact cast from the as-milled suspension, the layer close to the mold does not differ from the above suspension.

The pores are of the size of the elementary powder particles. Krell et al. claimed that one of the indicators for successful homogeneous processing is that the average pore size is approximately 1/5 of the particle size.[13] Therefore the homogeneity of both of the green-compacts is not optimal.

6 Summary and Conclusions

The previously assumed microstructure of a flocculated suspension was confirmed by cryo-SEM of vitrified suspensions, and correlated with flocculation using rheology measurements. Flocculation is affected by several parameters of the suspension. Some of the most critical parameters include additives such as dispersing agents, solid-loading of the suspension, particle size distribution of the powder, and aging. Flocculation can also be caused by either excess or deficient amount of dispersant, or a high molecular weight of the dispersant. In this study an excess amount of polymeric dispersant is probably the source of particle bridging and flocculation.

The initial spinel powder used in this study was heavily agglomerated. Ball-milling was only successful in breaking up the soft agglomerates. The residual hard agglomerates had an average diameter of 170 nm, and were composed of several elementary particles. The structures in the original suspension are flocs, hundreds of nanometers in diameter, and not 170nm as indicated from light scattering. The source of this discrepancy is the requirement for dilute suspensions for SLS, making its use limited for characterizing suspensions at solid concentrations relevant for slip casting.

The powder was characterized to have an isoelectric point at pH=11.8. Acidity (pH) adjustments alone did not disperse the powder in water, although the electric repulsion was high enough according to zeta potential measurements. Polyacrylate based dispersants of the group tested, shifted the isoelectric point to pH=3.3. Zeta potential measurements, which also must be conducted on relatively dilute suspensions, only provide information on electrostatic forces. As a result, the suspension was flocculated, even though the zeta potential measured for the dilute suspension at a pH above 10 predicts good stability.

The investigated spinel suspension was rheologically characterized to be pseudo-plastic, and the aged suspension is also thixotropic. An aging phenomenon of increasing flocculation with time was observed for the sub-micron length-scale powders, requiring an increased shear stress to separate the particles.

The techniques described above, augmented by cryo-SEM, can be applied to

characterize other ceramic suspensions, and optimize the suspension for specific processing. The advantage of cryo-SEM (combined with viscosity measurements) is that it can be conducted on suspensions having a solid concentration applicable to slip casting, providing direct imaging of the micro-structure of the original suspension used for casting.

The green density and pore size measurements shed some light on the casting process of spinel green compacts. If the casting process lasts long enough, the slurry is flocculated before the green body is formed. Therefore, neither density nor pore size distribution analysis can discern between green compacts created by as-milled suspensions and the ones created by aged suspensions.

Although the microstructure expected for a flocculated suspension is inhomogeneous, the obtained microstructure is quite homogeneous, with a narrow pore size distribution. This is probably a result of the high solid-loading of the suspension, which resulted in a high green density and overcame the predicted inhomogeneous microstructure.

7 Suggested Future Research Directions

❖ Characterization and comparison of spinel powders, produced by different methods. Different powder production methods may affect the particle shape, the particle size distribution, the tendency to agglomerate, the surface chemistry, etc. For example, powder production method based on FSP (flame spray pyrolysis) usually leads to more spherical particles than those obtained by the alum-based process (the production method of the powder investigated in this research).

❖ Optimization of composition in terms of solid-loading and dispersant concentration of the investigated suspension, based on imaging using cryo-SEM.

❖ Comparison between the investigated suspension and suspensions based on different dispersants.

❖ Characterization of additional ceramic suspensions, YAG for example, using cryo-SEM.

References

[1] S. J. Schneider, "Engineering Properties of Multicomponents and Multiphase Oxides"; pp. 765-6 in *Engineered Materials Handbook, vol.4: Ceramics and Glasses*, edited by S. R. Lampman, M. S. Woods and T. B. Zorc ASM International, USA, 1991.

[2] C. B. Carter and M. G. Norton, "Complex Crystal and Glass Structures"; pp. 100-2 in *Ceramic Materials Science and Engineering*, Springer, New York, NY, 2007.

[3] J.A. Savage, "Preparation and Properties of Hard Crystalline Materials for Optical Applications - A Review," *J. Cryst. Growth*, **113** [3-4] 698-715 (1991).

[4] D. C. Harris, "Thermal Properties"; pp. 135 and "Appendix C: Optical Properties of Infrared Materials"; pp. 354 in *Materials for Infrared Windows and Domes – Properties and Performances*, edited by D. C. Harris. SPIE – Optical Engineering Press, Bellingham, WA, 1999.

[5] A. Krell, J. Klimke and T. Hutzler, "Advanced Spinel and Sub-μm Al_2O_3 for Transparent Armour Applications," *J. Eur. Ceram. Soc.*, **29** [2] 275-81 (2009).

[6] A. Krell, T. Hutzler, J. Klimke and A. Potthoff, "Fine-Grained Transparent Spinel Windows by the Processing of Different Nanopowders," *J. Am. Ceram. Soc.*, **93** [9] 2656-66 (2010).

[7] K. Maca, M. Trunec and R. Chmelik, "Processing and Properties of Fine-Grained Transparent $MgAl_2O_4$ Ceramics," *Ceramics-Silikaty*, **51** [2] 94-7 (2007).

[8] N. Benameur, G. Bernard-Granger, A. Addad, S. Raffy, and C. Guizard, "Sintering Analysis of a Fine-Grained Alumina–Magnesia Spinel Powder," *J. Am. Ceram. Soc.*, **94** [5] 1388–96 (2011).

[9] I. Ganesh, "Aqueous Slip Casting of $MgAl_2O_4$ Spinel Powder," *Bull. Mater. Sci.*, **34** [2] 327–35 (2011).

[10] I. Ganesh, S. M. Olhero, P. M. C. Torres, and J. M. F. Ferreira, "Gelcasting of Magnesium Aluminate Spinel Powder," *J. Am. Ceram. Soc.*, **92** [2] 350–357 (2009).

[11] J. Binner and B. Vaidhyanathan "Processing of bulk nanostructured ceramics," *J. Eur. Ceram. Soc.*, **28** [7] 1329-39 (2008).

[12] J. A. Lewis, "Colloidal Processing of Ceramics," *J. Am. Ceram. Soc.,* **83** [10] 2341–59 (2000).

[13] A. Krell and J. Klimke, "Effects of the Homogeneity of Particle Coordination on Solid-State Sintering of Transparent Alumina," *J. Am. Ceram. Soc.,* **89** [6] 1985–92 (2006).

[14] Y. Hotta, T. Tsugoshi, T. Nagaoka, M. Yasuoka, K. Nakamura and K. Watari, "Effect of Oligosaccharide Alcohol Addition to Alumina Slurry and Translucent Alumina Produced by Slip Casting," *J. Am. Ceram. Soc.*, **86** [5] 755-60 (2003).

[15] D. J. Shanefield, "Appendix II – Words Used in Colloid Science"; pp. 297-8 in *Organic Additives and Ceramic Processing, 2nd edition*, Kluwer Academic Publishers, Massachusetts, 1999.

[16] R. H. French "Origins and Applications of London Dispersion Forces and Hamaker Constants in Ceramics," *J. Am. Ceram. Soc.*, **83** [9] 2117-46 (2000).

[17] G. Y. Onoda, Jr., L. L. Hench, R. E. Misyler, D. J. Shanefield and R. B. Runk, "Physical Characterization Terminology"; pp. 36-37 and "Tape Casting of Ceramics"; pp. 418-419 in *Ceramic Processing before Firing*, edited by G. Y. Onoda, Jr. and L. L. Hench. Wiely-Interscience, Gainesville, 1978.

[18] K. Sato, H. Yilmaz, Y. Hotta, A. Ijuin and K. Watari, "Dispersion of Ceramic Particles in Aqueous Media with Surface-Grafted Dispersant," *J. Am. Ceram. Soc.*, **92** [1] 256–9 (2009).

[19] R. Xu, "Laser Diffraction"; pp. 111-2 in *Particle characterization: Light Scattering Methods*, edited by B. Scarlett, Kluwer Academic Publishers, Miami, 2002.

[20] M. Kosmulski, "Compilation of PZC and IEP of sparingly soluble metal oxides and hydroxides from literature", *Adv Colloid Interface Sci.,* **152** [1-2] 14-25 (2009).

[21] T. L. Doane, C. Chuang, R. J. Hill and C. Burda, "Nanoparticle ζ-Potentials," *Acc. Chem. Res.,* doi: 10.1021/ar200113c.

[22] J. Cesarano and I. A. Aksay, "Processing of Highly Concentrated Aqueous α-Alumina Suspensions Stabilized with Polyelectolytes," *J. Am. Ceram. Soc.*, **71** [12] 1062-67 (1988).

[23] S. Vallar, D. Houivet, J. El Fallah, D. Kervadec and J.-M. Haussonne, "Oxide Slurries Stability and Powders Dispersion: Optimization with Zeta Potential and Rheological Measurements," *J. Eur. Ceram. Soc.*, **19** [6-7] 1017-21 (1999).

[24] O. Lyckfeldt, L. Palmqvist and E. Carlstrom, "Stabilization of Alumina with Polyelectrolyte and Comb Copolymer in Solvent Mixtures of Water and Alcohols," *J. Eur. Ceram. Soc.*, **29** [6] 1069-76 (2009).

[25] S. M. Olhero, I. Ganesh, P. M.C. Torres and J. M.F. Ferreira, "Surface Passivation of $MgAl_2O_3$ Spinel Powder by Chemisorbing H_3PO_4 for an Easy Aqueous Processing," *Langmuir* **24** [17] 9525-30 (2008).

[26] M. S. Zbik, R. St.C. Smart and G. E. Morris, "Kaolinite Flocculation Structure," *J. Colloid Interface Sci.*, **328** [1] 73–80 (2008).

[27] A. Lasalle, C. Guizard, S. Deville, F. Rossignol and P. Carles, "Investigating the Dispersion State of Alumina Suspensions: Contribution of Cryo-Field-Emission Gun Scanning Electron Microscopy Characterizations," *J. Am. Ceram. Soc.*, **94** [1] 244–9 (2011).

[28] L. Muscariello, F. Rosso, G. Marino, A. Giordano,M. Barbarisi, G. Cafiero and A. Barbarisi, ”A Critical Overview of ESEM Applications in the Biological Field,” *J. Cell. Physiol.*, **205** 328–34 (2005).

[29] A. Bogner, P.H. Jouneau, G. Thollet, D. Basset and C. Gauthier, “A history of scanning electron microscopy developments: Towards ‘‘wet-STEM’’ imaging,” *Micron* **38** 390–401(2007).

[30] K. Tiede, S. P. Tear, H. David and A. B.A. Boxall, “Imaging of engineered nanoparticles and their aggregates under fully liquid conditions in environmental matrices,” *Water Research*, **43** 3335-43 (2009).

[31] G. Venkiteela and Z. Sun, “In situ observation of cement particle growth during setting,” *Cement & Concrete Composites*, **32** 211–8 (2010).

[32] M. A. Whitelaw-Weckert, E. S. Whitelaw, S. Y. Rogiers, L. Quirk, A. C. Clark and C. X. Huang, "Bacterial Inflorescence Rot of Grapevine Caused by Pseudomonas Syringae pv. Syringae," *Plant Pathology* **60** [2] 325–37 (2011).

[33] F. M. Menger, H. Zhang, K. L. Caran, V. A. Seredyuk and R. P. Apkarian, ”Gemini-Induced Columnar Jointing in Vitreous Ice. Cryo-HRSEM as a Tool for

Discovering New Colloidal Morphologies," *J. Am. Chem. Soc.*, **124** [7] 1140-1 (2002).

[34] H. Luo, L.E. Scriven and L. F. Francis, "Cryo-SEM Studies of Latex/Ceramic Nanoparticle Coating Microstructure Development," *J. Colloid Interface Sci.*, **316** [2] 500–9 (2007).

[35] L. Omer, S. Ruthstein, D. Goldfarb and Y. Talmon, "High-Resolution Cryogenic-Electron Microscopry Reveals Details of a Hexagonal-to-Bicontinuous Cubic Phase Transition in Mesoporous Silica Synthesis," *J. Am. Chem. Soc.*, **131** [34] 12466-73 (2009).

[36] H. M. Wyss, M. Hutter, M. Muller, L. P. Meier and L. J. Gauckler, "Quantification of Microstructures in Stable and Gelated Suspensions from Cryo-SEM," *J. Colloid Interface Sci.*, **248** [2] 340–6 (2002).

[37] M. Zbik, "SEM Evidence of Structural Re-Arrangement from Gelling to Aggregation in Birdwood Kaolinite," *Colloids Surf. A: Physicochem. Eng. Aspects* **287** 191–6 (2006).

[38] H. Ge, W. J. Suszynski, H. T. Davis and L. E. Scriven, "New controlled environment vitrification system for preparing wet samples for cryo-SEM," *J. Microsc.*, **229** [1] 115-26 (2008).

[39] L. Issman and Y. Talmon, "Cryo-SEM Specimen Preparation under Controlled Temperature and Concentration Conditions," *J. Microsc.*, **246** [1] 60–9 (2012).

[40] P. A. Webb and C. Orr, "Pore Structure by Mercury Intrusion Porosimetry (MIP)"; pp. 155-8 in *Analytical Methods in Fine Particle Technology*, Micromeritics Instrument Corporation, Norcross, 1997.

[41] ASTM Standard D2196, 2005 "Test Methods for Rheological Properties of Non Newtonian Materials by Rotational (Brookfield type) Viscometer," *ASTM International*, West Conshohocken, PA, 2005, doi: 10.1520/D2196-05, www.astm.org.

[42] Y. Qi, E. Kesselman, D. J. Hart, Y. Talmon, A. Mateo and J. L. Zakin, "Comparison of Oleyl and Elaidyl Isomer Surfactant–Counterion Systems in Drag Reduction, Rheological Properties and Nanostructure," *J. Colloid Interface Sci.*, **354** [2] 691–9 (2011).

[43] J. Du, R. A. Pushkarova and R. St.C. Smart, "A Cryo-SEM Study of Aggregate and Floc Structure Changes During Clay Settling and Raking Processes," *Int. J. Miner. Process.*, **93** [1] 66–72 (2009).

[44] J. Cesarano and I. A. Aksay, "Processing of Highly Concentrated Aqueous α-Alumina Suspensions Stabilized with Polyelectolytes," *J. Am. Ceram. Soc.*, **71** [12] 1062-67 (1988).

[45] A. Saberi, F. Golestani-Fard, M. Willert-Porada, R. Simon, T. Gerdes and H. Sarpoolaky, "Improving the Quality of Nanocrystalline $MgAl_2O_4$ Spinel Coating on Graphite by a Prior Oxidation Treatment on the Graphite Surface," *J. Eur. Ceram. Soc.*, 28 [10] 2011-7 (2008).

[46] H. Zhang, X. Jia, Z. Liu and Z. Li, "The Low Temperature Preparation of Nanocrystalline $MgAl_2O_4$ Spinel by Citrate Sol–Gel Process," *Mat. Lett.*, **58** [10] 1625-8 (2004).

[47] C. A. Gutiérrez and R. Moreno, "Preventing ageing on Al_2O_3 casting slips dispersed with polyelectrolytes," *J. Mat. Sci.* **35** [23] 5867–72 (2000).

[48] T. L. Doane, C. Chuang, R. J. Hill and C. Burda, "Nanoparticle ζ-Potentials," *Acc. Chem. Res.*, doi: 10.1021/ar200113c.

[49] M. N. Rahaman, "Science of Colloidal Processing"; pp. 210-2 in *Ceramic Processing and Sintering*, edited by M. N. Rahaman. Taylor and Francis, Missouri, 2003.

[50] A. S. Dukhin and P. J. Goetz, "New developments in acoustic and electroacoustic spectroscopy for characterizing concentrated dispersions," Colloids Surf. A: Physicochem. Eng. Aspects **192** 267–306 (2001).

[51] M. Michalkova, K. Ghillanyova and D. Galusek, "The influence of solid loading in suspensions of a submicrometric alumina powder on green and sintered pressure filtrated samples," *Ceram. Int.* **36** [1] 385–90 (2010).

[52] J.A Lewis, "Direct-write assembly of ceramics from colloidal inks," *Current Opinion in Solid State and Materials Science*, **6** [3] 245-50 (2002).

[53] S. K. Friedlander "Collision and Coagulation"; pp 200-2 in *Smoke, Dust, and Haze – Fundamentals of Aerosol Dynamics 2nd ed.*, edited by S. K. Friedlander. Oxford University Press, NY, 2000.

[54] I. C. Tse, K. Swetland, M. L. Weber-Shirk and L. W. Lion, "Fluid shear influences on the performance of hydraulic flocculation systems," *Water Research* **45** [17] 5412-8 (2011).

[55] B. P. Singh, R. Menchavez, M. Fuji and M. Takahashi, "Characterization of concentrated colloidal ceramics suspension: A new approach," *J. Colloid Interface Sci.* **300** 163–8 (2006).

פורוזימטרייה של הגופים הירוקים מהווה נדבך נוסף באפיון המיקרו-מבנה המוביל להיווצרות הגוף המסונטר. פילוג גודל הנקבוביות של הגוף הירוק שנוצר מתרחיף רגיל דומה מאוד לפילוג של זה שנוצר מתרחיף מיושן.

מסקנות

דימות ישיר במיקרוסקופ אלקטרונים סורק, בטמפרטורות נמוכות היא שיטת אפיון המתאימה לתרחיפים קראמיים בעלי תכולת מוצקים גבוהה. המחקר מראה שהשימוש במיקרוסקופ הנ"ל מספק הבנה טובה יותר של המיקרו-מבנה של התרחיף המרוכז, בפרט בהשוואה לשיטות שלא ניתנות ליישום בתרחיפים מרוכזים. שיטת האפיון הנ"ל מסוגלת לתת מענה גם לאפיון תרחיפים בריכוזים שבהם שיטות אחרות, דוגמת מדידת פילוג גודל חלקיקים ע"י פיזור אור, לא ניתנות ליישום.

מדידת פוטנציאל זיטה בתרחיף מדולל, אין בה די כדי להעיד על יציבות התרחיף הרגיל, וראיה לכך היא תהליך הפלוקולציה שהתרחיף עובר, על אף שמירה על רמת חומציות המאפשרת ייצוב חשמלי.

תרחיף הספינל שאופיין עובר פלוקולציה, הגוברת עם התיישנותו. על כן, התרחיף לא ניוטוני, והתנהגותו הראולוגית ניתנת לסיווג כפסאודו-פלסטית. התרחיף המיושן מראה התנהגות תיקסוטרופית – ירידה בצמיגות לאורך זמן, בהפעלת כוח גזירה בקצב קבוע, אך בסופו של דבר, צמיגותו עולה בהפעלת זרימת גזירה למינרית.

מתוצאות הפורוזימטרייה ניתן להסיק שהגופים היצוקים מתייבשים בקצב איטי, ועל כן התרחיף שבתבנית היציקה עובר התיישנות ופלוקולציה, במידה דומה לתרחיף שעבר התיישנות מכוונת. על כן, בבואנו לחקור את התרחיף המיועד ליציקה ולהשליך ממבנהו על מבנה הגוף הירוק, יש לחקור גם את התרחיף המיושן.

תוצאות

מערכת המודל אותה חקרנו היא תרחיף מימי של אבקת ספינל. התרחיף המיועד ליציקה הוא בעל תכולת מוצקים גבוהה, ולכן נדרש לדללו על מנת לבצע חלק ניכר משיטות האפיון המוכרות. הגודל הממוצע של החלקיק הראשוני ניתן לחישוב על פי תוצאת מדידת שטח הפנים הספציפי של האבקה; ערכו עומד על כ-55 ננומטר. מדידת פילוג גודל החלקיקים לפני ואחרי טחינה מראה שהחלקיקים עודנו, כלומר בוצעה דה-אגלומרציה, אבל לא באופן מוחלט. לאחר הטחינה נותרים אגלומרטים קשים שגודלם נע סביב 170 ננומטר. בדימות ישיר של התרחיף המדולל, ניתן לראות את המבנים האלה: אגלומרטים בגודל של 150 עד 200 ננומטר, המורכבים מחלקיקים ראשוניים בגודל של עשרות ננומטרים.

הנקודה האיזו-אלקטרית של אבקת הספינל (ללא מתרחף) מצויה ברמת חומציות של כ-11.8. למתרחף אופי חומצי חלש. על מנת לקבל משיכה בינו לבין האבקה, יש לעבוד ברמת חומציות גבוהה מספיק כדי לגרום לדיסוציאציה של האתרים הפונקציונליים (יצירת אתרים בעלי מטען שלילי), ובמקביל לשמור על רמת חומציות כזו שתותיר את פני שטח האבקה חיוביים (מתחת לנקודה האיזו-אלקטרית). נקודת העבודה שנבחרה היא סביב pH=10.
הנקודה האיזו-אלקטרית של תרחיף הספינל מצויה ברמת חומציות של כ-3.3 ומכאן שעבודה ברמת החומציות שנבחרה, צפויה להיות "בטוחה" מבחינת ייצוב חשמלי. עם זאת, מכיוון שמדידת פוטנציאל זיטה מתבצעת בתנאים של תרחיף דליל, ולא לוקחת בחשבון אינטראקציות מרחביות, לא ניתן ללמוד על מידת היציבות של התרחיף מנתון זה בלבד.

מדידת צמיגות בקצב גזירה משתנה הראתה שככל שקצב הגזירה עולה, צמיגות התרחיף יורדת, כלומר התרחיף מתנהג כמערכת פסאודו-פלסטית. מדידת צמיגות לאורך זמן, בהפעלת קצב גזירה קבוע, הראתה שצמיגות התרחיף תחילה יורדת, ולאחר מכן מתחילה לעלות. התנהגות דומה, אם כי קיצונית יותר, נצפתה גם בתרחיף המיושן. התנהגות זו ניתנת להסבר בהתייחס לאינטראקציות הפעולות בין החלקיקים בתרחיף, במהלך המדידה: בזמן שהתרחיף במנוחה, צמיגותו עולה עקב פלוקולציה, היווצרות צברים (flocs) של חלקיקים בתרחיף, בגלל תנועה בראונית וכוחות משיכה. עם תחילת הפעלת מאמצי גזירה, נגרמת דה-פלוקולציה (פירוק הצברים). לאחר מספר דקות, קצב היווצרות הצברים גובר על קצב פירוקם, ונוצרת רה-פלוקולציה, עקב תנועתם היחסית של החלקיקים תחת זרימת גזירה למינרית. הצברים הנוצרים במנגנון זה חזקים וצפופים יותר. דימות ישיר של התרחיף הרגיל, בהשוואה לתרחיף המיושן, מוכיח שהפלוקולציה באחרון מוגברת. מעבר לכך, הדימות הישיר מספק מידע על המיקרו-מבנה של התרחיף, על גודל הצברים ועל צפיפותם.

מדידות ראולוגיות

תכונותיו הראולוגיות של התרחיף יכולות להעיד על יציבותו ועל המיקרו-מבנה שלו. ניתן לסווג את המערכות הזורמות למערכות ניוטוניות – מערכות שצמיגותן אינה תלויה בזמן ובקצב הגזירה, ולמערכות לא ניוטוניות – בהן יש תלות כלשהי של הצמיגות בפרמטרים אלה. תרחיף קראמי בעל תכולת מוצקים גבוהה, צפוי להיות לא ניוטוני ולכן נבדקו שני הפרמטרים: נמדדה צמיגות התרחיף המיועד ליציקה, באמצעות מד צמיגות, בקצבי גזירה משתנים. כן נמדדה צמיגות התרחיף המיושן לאורך זמן, תוך הפעלת קצב גזירה קבוע.

אפיון הגוף הירוק

כפי שצוין לעיל, המיקרו-מבנה של התרחיף משפיע על המיקרו-מבנה של הגוף הירוק, והוא בתורו, משפיע על התקדמות הסינטור. יש חשיבות לצפיפות הגוף הירוק, ויותר מכך לגודל ופילוג הנקבוביות בגוף הירוק, שכן גודל נקבוביות אחיד מסייע לציפוף אחיד. על כן נמדדה צפיפות הגוף הירוק בשיטת ארכימדס. פילוג גודל הנקבוביות נמדד בשיטת פורוזימטריית כספית: החדרת כספית לדגם בלחץ עולה, ומדידת נפח הכספית שחדרה דרך הנקבוביות כתלות בלחץ. ניתן לחשב את פילוג גודל הנקבוביות בהתבסס על הקשר בין מתח הפנים של הכספית לבין הלחץ הנדרש כדי להחדירה לנקבוביות. על מנת ללמוד על השפעת ההתיישנות של התרחיף, נערכה השוואה בין פילוג גודל הנקבוביות של שני גופים ירוקים שהוכנו בשיטה שונה: האחד נוצק על גבי מצע יבש כלומר נוצר מתרחיף רגיל, והשני נוצק על מצע ספוג במים, ורק לאחר שהתרחיף עבר התיישנות, המצע ייובש, והגוף החל להיווצר, כלומר נוצר מתרחיף מיושן.

שיטות המחקר

<u>הכנת תרחיף</u>

הכנו תרחיף ספינל מימי, בעל תכולת מוצקים של 60% משקלי, תוך שימוש במתרחף פולימרי. התרחיף נטחן למשך 24 שעות במטחנת כדוריות, לשם קבלת תרחיף הומוגני ופירוק אגלומרטים. התרחיף אופיין בשלושה מצבים שונים: 1) רגיל – התרחיף המיועד ליציקה, מיד לאחר טחינה; 2) מיושן – לאחר המתנה למשך פרק זמן מוגדר, ללא טחינה או ערבוב, מתום הטחינה; 3) מהול – לאחר טחינה במצב המרוכז, בוצע מיהול ע"י הוספת מים מזוקקים. בנוסף, התרחיף הרגיל נוצק על גבי מצע נקבובי ובוצע אפיון של הגוף הירוק, שנוצר לאחר ספיגת המים דרך המצע.

<u>דימות ישיר באמצעות מיקרוסקופיית אלקטרונים סורקת בטמפרטורות נמוכות</u>

מיקרוסקופ האלקטרונים הסורק מאפשר התבוננות במבנים בסדרי גודל תת-מיקרוניים ואף ננומטריים, הודות לכושר ההפרדה הגבוה שלו. מכיוון שהדגם נמצא בתא ואקום, לא ניתן להתבונן בדוגמאות רטובות. בשיטה של דימות ישיר בטמפרטורות נמוכות, הדוגמה הנוזלית עוברת ויטריפיקציה ע"י קירור מהיר. הויטריפיקציה מובילה לקיבוע פיזיקלי ושימור של המיקרו-מבנה, תוך הורדת לחץ האדים של הדוגמה, כך שתתאפשר הכנסתה לתא הואקום של המיקרוסקופ, מבלי שתעבור המראה. לאחר שלב הקירור המהיר, הדוגמה נשמרת בטמפרטורה קריוגנית, ובטמפרטורה זו היא גם מאופיינת במיקרוסקופ.

<u>מדידת פילוג גודל חלקיקים בשיטת פיזור אור</u>

אלומת לייזר מוקרנת לעבר טווח המכיל חלקיקים מרחפים. האלומה פוגעת בחלקיקים ומתפזרת בזוויות ועוצמות שונות, כתלות בגודל החלקיקים וריכוזם בתרחיף. מערך של חיישנים קולט את האור המתפזר, ואלגוריתם מתמטי קושר בין סך האותות הנקלטים לגלאים לבין התפלגות הגדלים של החלקיקים, שפיזרו את האור. שיטה זו מחייבת שימוש בתווך שקוף ובריכוז חלקיקים נמוך, כדי להימנע מפיזורים חוזרים, לכן מתבצעת בתרחיף דליל פי 10000-1000 מהתרחיף המיועד ליציקה.

<u>מדידת פוטנציאל זיטה</u>

פוטנציאל זיטה הוא הפוטנציאל החשמלי על פני השטח של חלקיק המצוי בתמיסה. סימן ועוצמת המטען, על פני השטח של חלקיקים בתרחיף, משפיעים על יציבות התרחיף ועל תכונותיו הראולוגיות. הנקודה שבה סך המטענים על החלקיק הוא 0, נקראת הנקודה האיזו-אלקטרית. בנקודה זו דחייה חשמלית מינימלית בין החלקיקים בתרחיף, וללא ייצוב מרחבי הם ייצמדו אלה לאלה, וישקעו. מדידת פוטנציאל זיטה בוצעה בשיטת פיזור אור, תוך כדי הפעלת מתח חילופין וקביעת המוביליות החשמלית של החלקיקים. גם מדידה זו מחייבת דילול של התרחיף המיועד ליציקה, עד לקבלת צלילות.

תקציר

רקע

המחקר עוסק בגישה חדשה לאפיון תרחיפים קראמיים, ע"י מיקרוסקופיית אלקטרונים סורקת בטמפרטורות נמוכות. הדגם עובר ויטריפיקציה, כלומר קיבוע המיקרו-מבנה של התרחיף על ידי קירור מהיר. הקירור המהיר מפחית ככל האפשר את היווצרות גבישי הקרח (מעבר של המים לפאזה גבישית), וכך נמנע שינוי של המיקרו-מבנה המקורי. לאחר תהליך הויטריפיקציה ניתן לבחון את המיקרו-מבנה של התרחיף במיקרוסקופ אלקטרונים סורק, בעל מחזיק דגם בטמפרטורה קריוגנית.

בשיטה זו בוצע אפיון של תרחיף מימי של אבקת ספינל – תמיסה מוצקה של מגנזיה ואלומינה (בעלת המבנה הגבישי הקרוי ספינל). תרחיף זה מיועד בתעשייה ליציקה על פני מצע נקבובי, היונק את המים ומותיר "גוף ירוק" – מבנה אבקתי דחוס, בעל חוזק מבני המאפשר המשך של ציפוף בתהליכי סינטור וחימום בלחיצה שוות-צירים. לאחר הסינטור לצפיפות מלאה, מתקבל גוף שקוף בעל חוזק מכאני גבוה וקשיות גבוהה. לגוף כזה יעילות בליסטית טובה, כלומר עמידות בפני פגיעת קליעים. שילוב היעילות הבליסטית עם השקיפות לאור הנראה ולאינפרה אדום, עושה את הספינל מתחרה מועדף כחומר לחלונות ממוגני ירי.

יש חשיבות עליונה להבנת המיקרו-מבנה של התרחיף, שכן מבנה הגוף הירוק מושפע רבות ממבנה התרחיף. מבנה הגוף הירוק משפיע, בתורו, על תהליך הסינטור. פיזור אחיד של החלקיקים בתרחיף מוביל למבנה אחיד של נקבוביות בגוף הירוק, המועיל להתקדמות הסינטור ולהשגת צפיפות מלאה, ללא חללים, שהוא התנאי ההכרחי לקבלת שקיפות ולהשגת תכונות מכאניות אופטימאליות.

מטרות

המטרה העיקרית של המחקר היא פיתוח שיטה ניסיונית לאפיון של תרחיף קראמי מימי בעל תכולת מוצקים גבוהה באמצעות מיקרוסקופ אלקטרונים סורק, הפועל בטמפרטורות קריוגניות. תרחיף מימי של אבקת ספינל נבחר כמערכת מודל. במקביל בוצע אפיון של התרחיף בשיטות קלאסיות נוספות, לשם השוואה וחיזוק תוצאות המיקרוסקופיה. מטרה נוספת של המחקר היא הבנת השפעת המיקרו-מבנה של התרחיף על מבנה הגוף הירוק. מטרה משנית של המחקר היא אפיון החלקיקים הראשוניים באבקה ואפיון מבנה האגלומרטים הקשים, שניהם בוצעו בתרחיף מהול.

המחקר נעשה בהנחיית פרופ' ווין קפלן, בפקולטה להנדסת חומרים
ופרופ' ישעיהו טלמון ויכין כהן, בפקולטה להנדסה כימית

אני מודה לרפאל בע"מ על התמיכה הכספית הנדיבה בהשתלמותי

אפיון תרחיפים קראמיים של אבקת ספינל ננומטרית

חיבור על מחקר

לשם מילוי חלקי של הדרישות לקבלת התואר
מגיסטר למדעים בהנדסת חומרים

תמר קדוש

הוגש לסנט הטכניון – מכון טכנולוגי לישראל

תמוז תשע"ב חיפה יולי 2012

אפיון תרחיפים קראמיים של אבקת ספינל ננומטרית

תמר קדוש